Supporting Information for

Donor–acceptor cross-conjugated phenazine macrocycle with large Stokes shift for "turn-on" sensing transition metal ions

Hui Li, Xuejie Zhang, Jianfeng Peng, Shuaijun Yang,* Riming Hu, Xuchuan Jiang*
(*Institute for Smart Materials & Engineering, University of Jinan, Shandong 250022, China*)
ism_yangsj@ujn.edu.cn (S. Y); ism_jiangxc@ujn.edu.cn (X. J)

Table of Contents

1. Experimental section

1.1 General

^{1}H-NMR and ^{13}C-NMR analyses were performed using a Bruker Avance III 600 spectrometer (^{1}H NMR, 600 MHz; ^{13}C NMR, 151 MHz). As internal references for ^{1}H-NMR and ^{13}C-NMR spectroscopy the signals of $CDCl_3$ were used and calculated relative to tetramethylsilane (TMS). The high resolution mass spectra were measured with a Thermo Fisher Scientific LTQ FTICR-MS instrument (DART positive ion mode). UV-Vis spectra were recorded using a UV-3600-plus spectrometer. Emission spectra were measured with an Edinburgh FLS1000 fluorimeter using a front-face solid sample configuration for solid samples. Absolute fluorescence quantum yields were obtained using an integrating sphere. All starting materials were purchased from commercial without further purification. Solvents used for optical record were spectroscopic grade. All reactions were carried out under an atmosphere of nitrogen unless otherwise noted.

1.2. Synthetic procedures and characterization data

Synthesis of compound LH-1

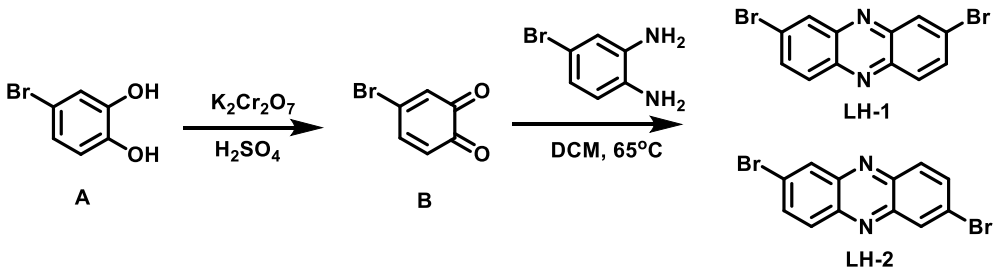

Potassium dichromate (3.53 g, 12.00 mmol, 2 eq), 4-bromo-1,2-benzenediol (1.128 g, 6.00 mmol, 1 eq), 36 mL of dilute sulfuric acid, and 200 mL of dichloromethane were added to a 500 mL round-bottomed flask. The reaction mixture was stirred at room temperature for 30 min. When the reaction was completed, the organic phase was isolated, and dried over anhydrous Na_2SO_4. To the dried organic solution were added 4-bromo-1,2-benzene diamine (1.116 g, 6.00 mmol, 1 eq) and 1 mL of acetic acid to accelerate the reaction rate. The reaction mixture was stirred at reflux for 10 h. Upon the completion of the reaction, the reaction mixture was extracted

with dichloromethane and washed with water. The organic layer was dried with anhydrous Na_2SO_4. After removing the solvent, the residue was purified by column chromatography on silica gel using ethyl acetate /petroleum ether (1/15, *V*/*V*) as eluent, yielding 0.20 g (9.83%) of **LH-1** as a yellow solid.

^{1}H-NMR (600 MHz, $CDCl_3$) δ 8.44 (d, J = 2.2 Hz, 2H), 8.11 (d, J = 9.4 Hz, 2H), 7.92 (dd, J = 9.3, 2.1 Hz, 2H) ppm. ^{13}C-NMR (151 MHz, $CDCl_3$) δ 144.0, 142.2, 134.8, 131.8, 131.1, 126.0 ppm. ES+-HRMS *m/z* (%): calcd. 338.8976 for $C_{12}H_7N_2Br_2$, $[M+H]^+$, found 338.8955.

Synthesis of compound LH-2

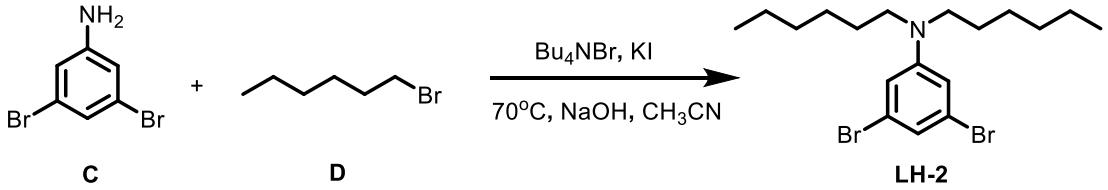

C **D** **LH-2**

3,5-dibromoaniline (6.414 g, 25.56 mmol, 1 eq), 1-bromohexane (1.128 g, 64.10 mmol, 2.5 eq), tetrabutylammonium bromide (0.824 g, 2.55 mmol, 0.1 eq), and potassium iodide (0.424 g, 2.55 mmol, 0.1 eq) were added to a 100 mL reaction vial. The air was exhausted and replaced three times with nitrogen, and then 20 ml of acetonitrile with sodium hydroxide (8.704 g, 217.60 mmol, 8.5 eq) was added under nitrogen protection. The reaction mixture was stirred at reflux for 22 h. Upon the completion of the reaction, the reaction mixture was extracted with ethyl acetate and washed with water. The organic layer was dried with anhydrous Na_2SO_4. After removing the solvents, the residue was purified by column chromatography on silica gel using dichloromethane/petroleum ether (1/10, *V*/*V*) as eluent, yielding 3.95 g (37.3%) of **LH-2** as a yellow oil.

^{1}H-NMR (600 MHz, $CDCl_3$) δ 6.86 (s, 1H), 6.63 (s, 2H), 3.21 (t, J = 3.8 Hz, 4H), 1.57 – 1.53 (m, 4H), 1.34 – 1.30 (m, 12H), 0.90 (t, J = 6.9 Hz, 6H) ppm. ^{13}C-NMR (151 MHz, $CDCl_3$) δ 150.1, 123.7, 120.1, 113.1, 51.1, 31.7, 27.0, 26.8, 22.8, 14.1 ppm. ES+-HRMS *m/z* (%): calcd. 420.0667 for $C_{18}H_{30}NBr_2$, $[M+H]^+$, found 420.0646.

Synthesis of compound LH-3

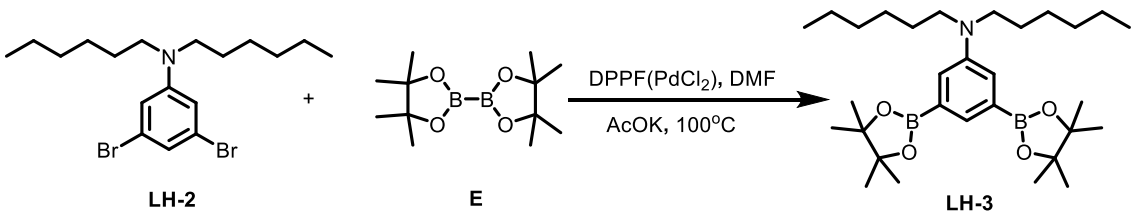

LH-2 (1.098 g, 2.63 mmol, 1 eq), bis(pinacolato)diboron (1.33 g, 5.26 mmol, 2 eq), potassium acetate (1.289 g, 13.15 mmol, 5 eq), and 1,1-bis(diphenylphosphino)ferrocene palladium(II) dichloride (0.19 g, 0.26 mmol, 0.1 eq) were added to 100 mL of a reaction flask. The air was exhausted and replaced three times with nitrogen, and then 25 mL of N,N-dimethylformamide was added under nitrogen protection. The reaction mixture (100°C, oil bath) was stirred for 20 h. Upon the completion of the reaction, the reaction mixture was extracted with dichloromethane and washed with water. The organic layer was dried with anhydrous Na_2SO_4. After removing the solvent, the residue was purified by column chromatography on silica gel using ethyl acetate /petroleum ether (1/10, *V*/*V*) as eluent, yielding 1.178 g (87.3%) of **LH-3** as a white solid.

^{1}H-NMR (600 MHz, $CDCl_3$) δ 7.56 (s, 1H), 7.21 (s, 2H), 3.30 (t, J = 7.6 Hz, 4H), 1.56 -1.54 (m, 4H), 1.32 (s, 36H), 0.91 (t, J = 6.9 Hz, 6H) ppm.^{13}C-NMR (151 MHz, $CDCl_3$) δ 147.4, 128.7, 121.9, 83.6, 50.7, 31.8, 27.2, 26.9, 25.0, 22.8, 14.2 ppm. ES+-HRMS *m/z* (%): calcd. 514.4161 for $C_{30}H_{54}B_2NO_4$, $[M+H]^+$, found 514.4278.

Synthesis of compound MC-1[1]

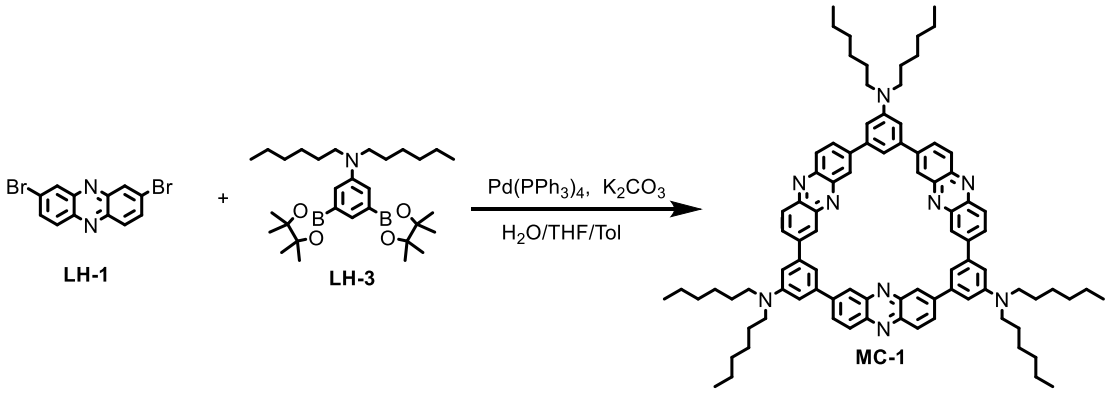

LH-1 (50 mg, 0.15 mmol, 1 eq.), anhydrous K_2CO_3 (123 mg, 0.89 mmol, 6 eq), and $Pd(PPh_3)_4$ (17.2 mg, 0.015 mmol, 0.1 eq) were added to a 100 mL reaction vial, and vacuumed to change nitrogen for three times. Reaction solvents (15 mL of

tetrahydrofuran, 6 mL of water, and 5 mL of toluene) were successively added. Toluene solution of **LH-3** (76.5 mg, 0.15 mmol, 1 eq, in 4 mL of toluene) was added dropwise using a microsyringe with the drop time of 30 min. The reaction mixture (100°C, oil bath) was stirred under nitrogen protection for 22 h. Upon the completion of the reaction, the reaction mixture was extracted with ethyl acetate and washed with water. The organic layer was dried with anhydrous Na_2SO_4. After removing the solvents, purified for isolation by preparative thin-layer chromatography on silica gel (eluent: petroleum ether: ethyl acetate = 4:1, *V*/*V*), yielding 4 mg (2.0%) of **MC-1** as an orange solid.

^{1}H-NMR (600 MHz, $CDCl_3$) δ 8.60 (d, J = 2.2 Hz, 6H), 8.35 (d, J = 9.0 Hz, 6H), 8.12 (d, J = 9.0 Hz, 6H), 7.48 (s, 3H), 7.04 (s, 6H), 3.47 (t, J = 7.7 Hz, 12H), 1.75-1.72 (m, 12H), 1.42-1.40 (m, 12H), 1.38-1.35 (m, 24H), 0.92 (t, J = 6.9 Hz, 18H). ^{13}C-NMR (151 MHz, $CDCl_3$) δ 149.2, 144.6, 144.4, 143.0, 142.4, 131.5, 130.0, 128.3, 127.3, 111.0, 51.5, 31.9, 27.4, 27.1, 22.9, 14.2. ES+-HRMS *m/z* (%): calcd. 1312.8493 for $C_{90}H_{106}N_9$, $[M+H]^+$, found 1312.8605.

Synthesis of compound SM-1

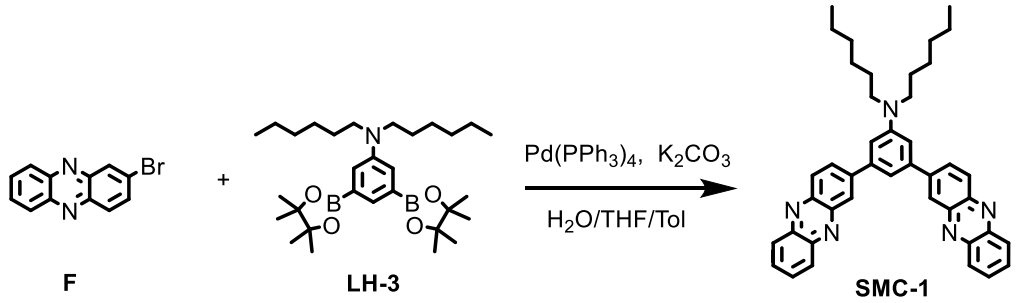

2-bromophenazine (50 mg, 195.31 mmol, 2 eq), **LH-3** (50 mg, 97.28 mmol, 1 eq), anhydrous K_2CO_3 (81 mg, 586.11 mmol, 6 eq), and $Pd(PPh_3)_4$ (11.28 mg, 9.73 mmol, 0.1 eq) were added to a 100 ml reaction flask, evacuated for nitrogen three times. Under the protection of nitrogen, 9 mL of tetrahydrofuran, 6 mL of water, and 9 mL of toluene were added sequentially, and the reaction mixture was stirred (100 °C, oil bath) for 20 h. Upon the completion of the reaction, the reaction mixture was extracted with ethyl acetate and washed with water. The organic layer was dried with anhydrous Na_2SO_4. After removing the solvent, purified for isolation by column chromatography on silca gel (eluent: petroleum ether: ethyl acetate = 4:1, *V*/*V*), yielding 75 mg (62.4%) of **SMC-**

1 as an orange solid.

^{1}H-NMR (600 MHz, $CDCl_3$) δ 8.56 (d, J = 2.2 Hz, 2H), 8.37 (d, J = 9.0 Hz, 2H), 8.29 – 8.24 (m, 6H), 7.87 – 7.86 (m, 4H), 7.51 (s, 1H), 7.17 (s, 2H), 3.49 (t, J = 7.7 Hz, 4H), 1.76 – 1.71 (m, 4H), 1.43 – 1.37 (m, 12H), 0.93 (t, J = 6.9 Hz, 6H) ppm.^{13}C-NMR (151 MHz, $CDCl_3$) δ 149.5, 144.1, 143.9, 143.6, 143.2, 141.6, 131.3, 130.8, 130.5, 130.1, 130.0, 129.7, 126.7, 114.5, 111.0, 51.4, 31.9, 27.5, 27.1, 22.9, 14.3 ppm. ES+-HRMS *m/z* (%): calcd. 618.3518 for $C_{42}H_{44}N_5$, $[M+H]^+$, found 618.3573.

Synthesis of compound SMC-2

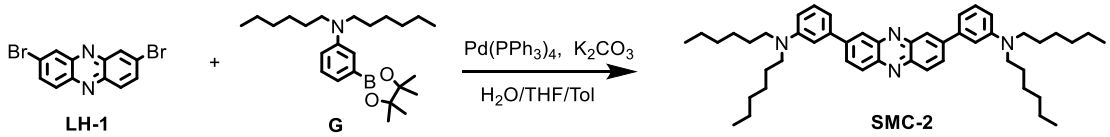

LH-1 (50 mg, 0.15 mmol, 1 eq), **G** (126 mg, 0.31 mmol, 2 eq), anhydrous K_2CO_3 (123 mg, 0.89 mmol, 6 eq), and $Pd(PPh_3)_4$ (17.20 mg, 0.015 mmol, 0.1 eq) were added to a 100 ml reaction vial. Under the protection of nitrogen, 9 ml of tetrahydrofuran, 6 ml of water, and 9 mL of toluene were sequentially added. The reaction mixture was stirred (100 °C, oil bath) for 18 h. Upon the completion of the reaction, the reaction mixture was extracted with ethyl acetate and washed with water. The organic layer was dried with anhydrous Na_2SO_4. After removing the solvent, purified for isolation by column chromatography on silica gel (eluent: petroleum ether: ethyl acetate = 4:1, as a *V*/*V*), yielding 68 mg (65.7%) of **SMC-2** as an orange solid.

^{1}H-NMR (600 MHz, $CDCl_3$) δ 8.45 (d, J = 2.2 Hz, 2H), 8.31 (d, J = 9.2 Hz, 2H), 8.15 (dd, J = 9.2, 2.0 Hz, 2H), 7.38 (t, J = 8.1 Hz, 2H), 7.08 – 7.07 (m, 4H), 6.76 – 6.73 (m, 2H), 3.38 (t, J = 7.7 Hz, 8H), 1.68 – 1.63 (m, 8H), 1.39 – 1.32 (m, 24H), 0.92 (t, J = 6.9 Hz, 12H) ppm. ^{13}C-NMR (151 MHz, $CDCl_3$) δ 148.9, 144.5, 144.2, 143.0, 140.7, 131.2, 130.1, 130.0, 126.2, 114.8, 112.1, 110.8, 51.3, 31.9, 27.4, 27.1, 22.9, 14.2 ppm. ES+-HRMS *m/z* (%): calcd. 699.5287 for $C_{48}H_{67}N_4$, $[M+H]^+$, found 699.5363.

Synthesis of compound SMC-3

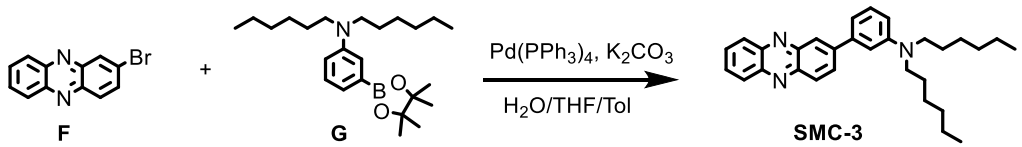

F (70 mg, 0.27 mmol, 1 eq), **G** (110 mg, 0.27 mmol, 1 eq), anhydrous K_2CO_3 (225 mg, 1.63 mmol, 6 eq), and $Pd(PPh_3)_4$ (31 mg, 0.027 mmol, 0.1 eq) were added in a 100 mL reaction flask, evacuate and replace nitrogen three times under nitrogen protection. Under the protection of nitrogen, 9 mL of tetrahydrofuran, 6 mL of water, and 9 mL of toluene were added sequentially, and the reaction mixture (100℃, oil bath) was stirred for 22 h. Upon the completion of the reaction, the reaction mixture was extracted with ethyl acetate and washed with water. The organic layer was dried with anhydrous Na_2SO_4. After removing the solvent, purified for isolation by column chromatography on silica gel (eluent: petroleum ether: ethyl acetate = 4:1, *V*/*V*), yielding 104 mg (86.5%) of **SMC-3** as an orange solid.

^{1}H-NMR (600 MHz, $CDCl_3$) δ 8.44 (d, J = 2.2 Hz, 1H), 8.30 – 8.25(m, 3H), 8.16 (dd, J = 9.0, 2.2 Hz, 1H), 7.85 – 7.83 (m, 2H), 7.38 (t, J = 4.0 Hz, 1H), 7.07 – 7.06 (m, 2H), 6.75 (dd, J = 8.3, 3.0 Hz, 1H), 3.37 (t, J = 7.74 Hz, 4H), 1.66 – 1.64 (m, 4H), 1.39 – 1.34 (m, 12H), 0.92 (t, J = 6.9 Hz, 6H) ppm. ^{13}C-NMR (151 MHz, $CDCl_3$) δ 148.9, 144.5, 143.9, 143.3, 143.1, 140.6, 131.5, 131.0, 130.3, 130.1, 129.8, 129.8, 129.6, 126.3, 114.8, 112.1, 110.8, 51.3, 31.9, 27.4, 27.0, 22.8, 14.2 ppm. ES+-HRMS *m/z* (%): calcd. 440.2987 for $C_{30}H_{38}N_3$, $[M+H]^+$, found 440.3042.

Synthesis of compound SMC-4

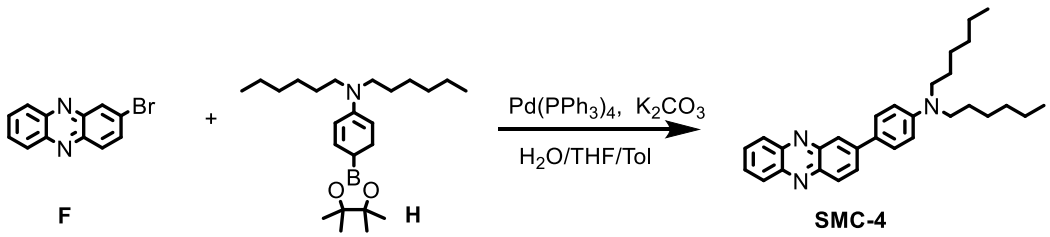

2-Bromophenazine (102 mg, 0.39 mmol, 1 eq), **H** (120 mg, 0.39 mmol, 1 eq), anhydrous K_2CO_3 (327 mg, 2.36 mmol, 6 eq), and $Pd(PPh_3)_4$ (45 mg, 0.039 mmol, 0.1 eq) were added in a 100 mL reaction flask. The reaction flask was evacuated to change nitrogen three times. Under the protection of nitrogen, 9 mL of tetrahydrofuran, 6 mL

of water, and 9 mL of toluene were added sequentially. The reaction mixture (100℃, oil bath) was stirred for 22 h. Upon the completion of the reaction, the reaction mixture was extracted with ethyl acetate and washed with water. The organic layer was dried with anhydrous Na_2SO_4. After removing the solvent, purified for isolation by column chromatography on silica gel (eluent: petroleum ether: ethyl acetate = 4:1, *V*/*V*), yielding 134 mg (76.5%) of **SMC-4** as an orange solid.

^{1}H-NMR (600 MHz, $CDCl_3$) δ 8.35 (d, J = 2.2 Hz, 1H), 8.24 – 8.21 (m, 3H), 8.18 (dd, J = 9.2, 2.0 Hz, 1H), 7.84 – 7.75 (m, 4H), 6.79 (d, J = 8.8 Hz, 2H), 3.36 (t, J = 7.2 Hz, 4H), 1.67 – 1.62 (m, 4H), 1.39 – 1.33 (m, 12H), 0.93 (t, J = 6.9 Hz, 6H) ppm. ^{13}C-NMR (151 MHz, $CDCl_3$) δ 148.7, 144.4, 144.0, 143.1, 143.0, 143.0, 130.8, 130.4, 129.8, 129.7, 129.5, 128.5, 125.3, 123.1, 112.1, 51.2, 31.7, 27.4, 27.0, 22.9, 14.3 ppm. ES+-HRMS *m/z* (%): calcd. 440.2987 for $C_{30}H_{38}N_3$, $[M+H]^+$, found 440.2987.

1.3 Preparation of the solutions for optical test and titration.

The solvents and concentrations used in this study: 1) **MC-1** and **SMC-1—4** solutions in dichloromethane at a concentration of 1.0×10^{-5} mol L^{-1}; 2) phloroglucinol (**THB**), 1,3,5-tribromobenzene (**TBB**), folic acid (**FA**), and cyanuric acid (**CA**) in acetonitrile at a concentration of 0.01 mol L^{-1}; 3) perchlorate salts (Fe^{3+}、Hg^{2+}、Pb^{2+}、Cu^{2+}、Fe^{2+}、Co^{2+}、Zn^{2+}、Ni^{2+}、Mn^{2+}) in acetonitrile at a concentration of 0.01 mol L^{-1}. The total added volume of metal ion solutions during the titration was controlled within the permissible error.

Detection method: The detection of Fe^{3+} was performed using a 1 cm path length quartz cell at room temperature with a fluorescence excitation wavelength of 388 nm. The selectivity for Fe^{3+} sensing of **MC-1** was conducted by adding 15 μL of the metal ions solutions (Fe^{3+}, Hg^{2+}, Pb^{2+}, Cu^{2+}, Fe^{2+}, Co^{2+}, Zn^{2+}, Ni^{2+}, and Mn^{2+} ions) at a concentration of 0.01 mol L^{-1} to 3 mL of the **MC-1** solution. The fluorescence emission or absorbance spectra were recorded after reaction for 1 min at room temperature. The same procedure was used for **SMC-1–4**.

The titration of Fe^{3+} ion in the presence of MC-1: 3 mL of **MC-1** was taken in the quartz cell, followed by the addition of 1–150 μL of Fe^{3+} ion solution, and the fluorescence intensity or absorbance was recorded after the 1 min of interaction time.

Job's plot: The complexation ratio of **MC-1** molecule with Fe^{3+} was determined by isomolar continuous change method (Job's plot). The total concentration of **MC-1** and Fe^{3+} in the solution system was fixed at 10^{-5}M, and the change of fluorescence intensity was determined by changing the composition ratio of **MC-1** and Fe^{3+}.[2]

2. Photophysical data of MC-1 and fragment molecules in solution.

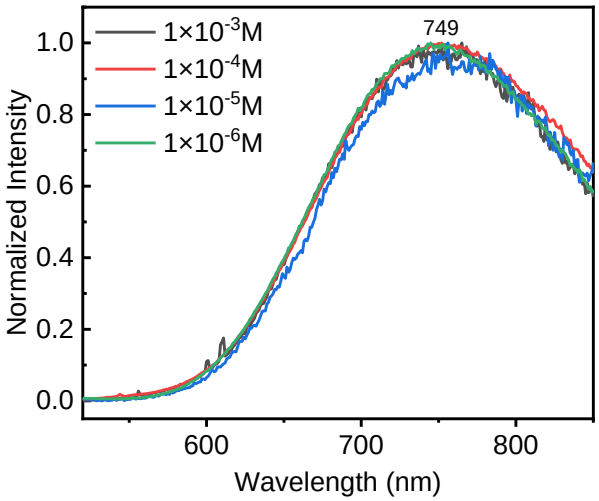

Figure S1. Emission spectra of **MC-1** in dichloromethane, were recorded at different concentrations.

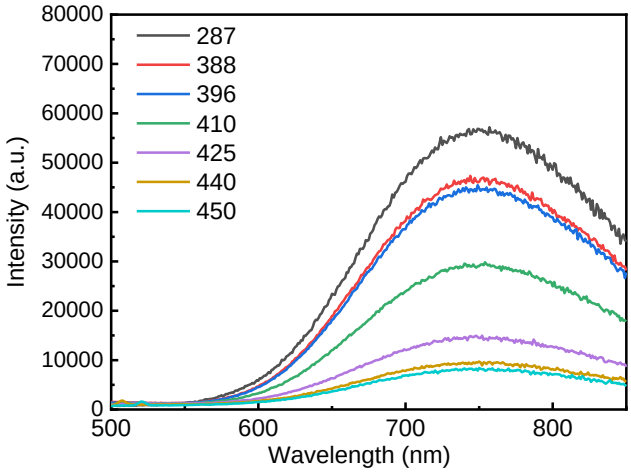

Figure S2. Emission spectra of **MC-1** in dichloromethane (1×10^{-5} mol L^{-1}, room temperature), were recorded at different excitation wavelengths (unit: nm).

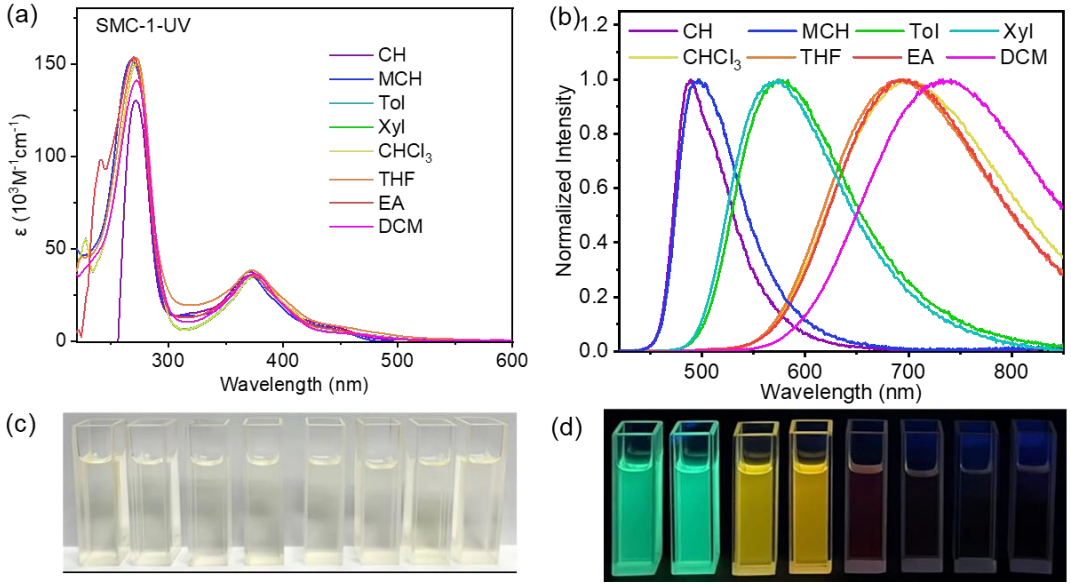

Figure S3. (a) Absorption and (b) Emission spectra of **SMC-1** in different solvents (1×10^{-5} M). (c,d) Images of solutions of **SMC-1** (1×10^{-5} M) in different solvents under ambient (c) and UV light (365 nm) (d). (from left to right cyclohexane (CH), methylcyclohexane (MCH), xylene (Xyl), toluene (Tol), tetrahydrofuran (THF), trichloromethane ($CHCl_3$), ethyl acetate (EA), dichloromethane (DCM))

Table S1 Photophysical data for **SMC-1** in different solvents

Solvents	λ_{ab} (nm)[a]	λ_{em} (nm)[a]	Φ_{fl} (%)[b]	τ (ns)[c]	Stokes shift (cm^{-1})[a]	FWHM (nm)[d]	K_r (10^7 s^{-1})[e]	K_{nr} (10^8 s^{-1})[f]
CH	370	500	17.12	4.26	7027	59.32	4.02	1.95
MCH	370	505	14.83	5.17	7225	71.38	2.87	1.65
Tol	375	575	18.57	8.79	9275	126.08	2.11	0.93
Xyl	376	571	10.07	7.78	9082	126.77	1.29	1.16
$CHCl_3$	374	693	3.04	2.63	12307	179.21	1.15	3.69
THF	374	692	4.74	4.46	12287	182.06	1.06	2.14
EA	373	699	0.92	2.90	12503	191.76	0.32	3.42
DCM	376	741	4.98	2.99	13100	210.14	1.67	3.18

[a]Measured in different solvents (1×10^{-5} M) at 300 K; [b]Absolute fluorescence quantum yield (Φ_{fl}) evaluated using an integrating sphere under air; [c]Fluorescence lifetimes (τ) measured under air at 300 K; [d]Full width at half-maximum (FWHM) of the fluorescence spectrum, given in wavelength; [e]Rate constant of fluorescence radiative decay: $K_r = \Phi_{fl}/\tau$; [f]Rate constant of nonradiative: $K_{nr} = (1 - \Phi_{fl})/\Phi_{fl}$

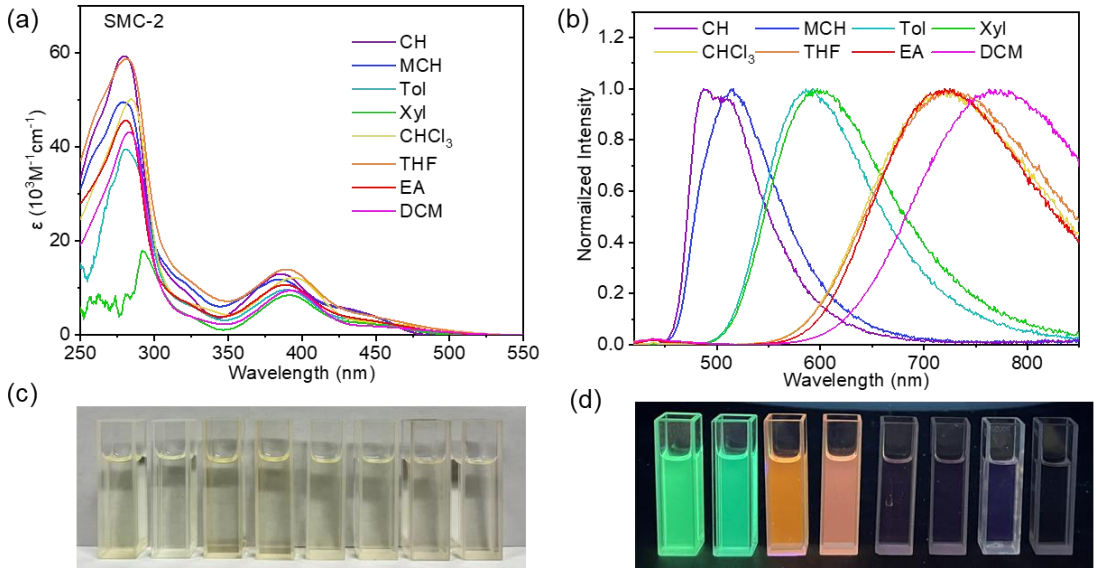

Figure S4. (a) Absorption and (b) Emission spectra of **SMC-2** in different solvents (1×10^{-5} M). (c,d) Images of solutions of **SMC-2** (1×10^{-5} M) in different solvents under ambient (c) and UV light (365 nm) (d).

Table S2 Photophysical data for **SMC-2** in different solvents

Solvents	λ_{ab} (nm)[a]	λ_{em} (nm)[a]	Φ_{fl} (%)[b]	τ (ns)[c]	Stokes shift (cm^{-1})[a]	FWHM (nm)[d]	K_r (10^7 s^{-1})[e]	K_{nr} (10^8 s^{-1})[f]
CH	386	516	18.69	17.71	6526	90.19	1.05	0.46
MCH	385	502	9.81	11.6	6053	78.82	0.84	0.79
Tol	390	591	12.61	11.16	8720	120.98	1.13	0.78
Xyl	390	600	9.58	9.17	8974	135.2	1.04	0.99
$CHCl_3$	388	722	< 0.1	3.26	11922	184.91	—	—
THF	389	722	8.72	4.06	11856	190.1	2.15	2.25
EA	388	729	< 0.1	3.34	12055	200.89	—	—
DCM	392	774	< 0.1	2.78	12590	220.3	—	—

[a]Measured in different solvents (1×10^{-5} M) at 300 K; [b]Absolute fluorescence quantum yield (Φ_{fl}) evaluated using an integrating sphere under air; [c]Fluorescence lifetimes (τ) measured under air at 300 K; [d]Full width at half-maximum (FWHM) of the fluorescence spectrum, given in wavelength; [e]Rate constant of fluorescence radiative decay: $K_r = \Phi_{fl}/\tau$; [f]Rate constant of nonradiative: $K_{nr} = (1 - \Phi_{fl})/\Phi_{fl}$

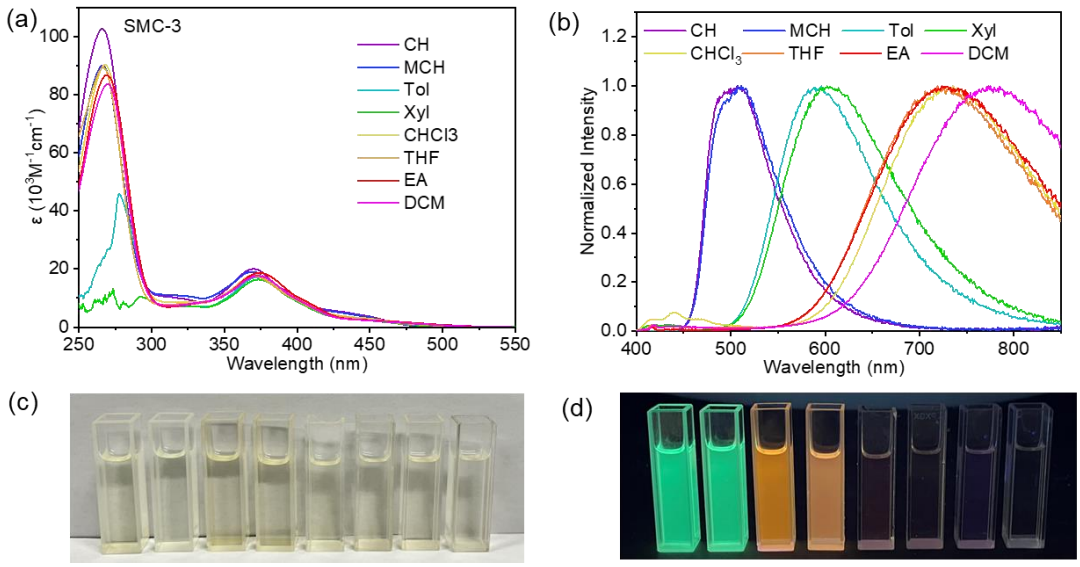

Figure S5. (a) Absorption and (b) Emission spectra of **SMC-3** in different solvents (1×10^{-5} M). (c,d) Images of solutions of **SMC-3** (1×10^{-5} M) in different solvents under ambient (c) and UV light (365 nm) (d).

Table S3 Photophysical data for **SMC-3** in different solvents

Solvents	λ_{ab} (nm)[a]	λ_{em} (nm)[a]	Φ_{fl} (%)[b]	τ (ns)[c]	Stokes shift (cm^{-1})[a]	FWHM (nm)[d]	K_r (10^7 s^{-1})[e]	K_{nr} (10^8 s^{-1})[f]
CH	369	504	9.2	7.39	7259	82.95	1.24	1.23
MCH	370	509	10.52	7.34	7380	88.08	1.43	1.22
Tol	373	593	9.79	9.77	9946	125.78	1.00	0.92
Xyl	373	607	12.17	7.57	10335	141.57	1.61	1.16
$CHCl_3$	374	731	0.5	3.06	13058	193.99	0.16	3.25
THF	371	730	2.17	3.77	13255	205.24	0.58	2.59
EA	371	734	< 0.1	3.04	13330	205.24	—	—
DCM	374	770	0.17	2.72	13751	221.6	0.06	3.68

[a]Measured in different solvents (1×10^{-5} M) at 300 K; [b]Absolute fluorescence quantum yield (Φ_{fl}) evaluated using an integrating sphere under air; [c]Fluorescence lifetimes (τ) measured under air at 300 K; [d]Full width at half-maximum (FWHM) of the fluorescence spectrum, given in wavelength; [e]Rate constant of fluorescence radiative decay: $K_r = \Phi_{fl}/\tau$; [f]Rate constant of nonradiative: $K_{nr} = (1 - \Phi_{fl})/\Phi_{fl}$

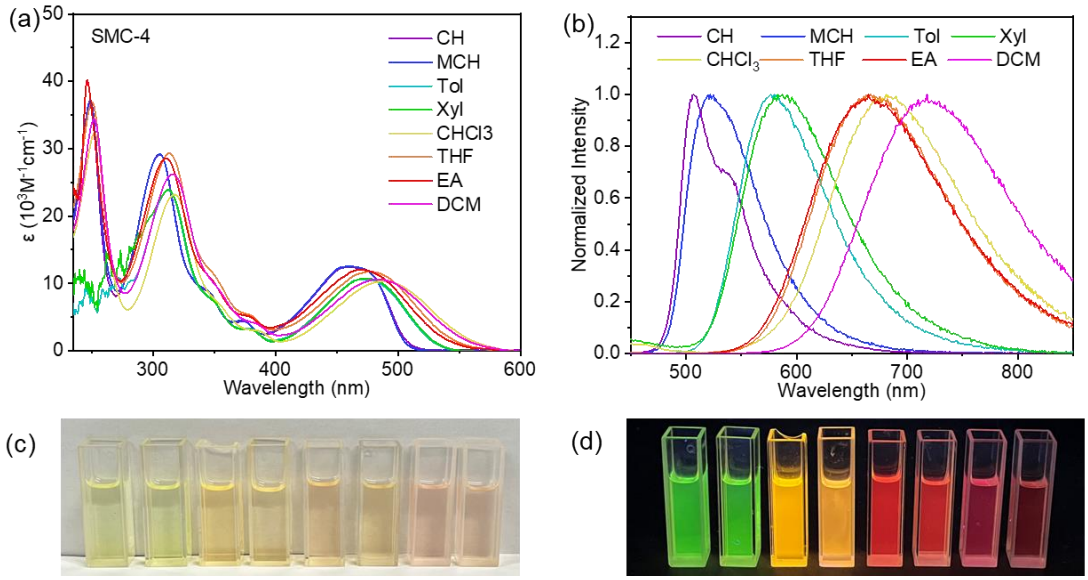

Figure S6. (a) Absorption and (b) Emission spectra of **SMC-4** in different solvents (1×10^{-5} M). (c,d) Images of solutions of **SMC-4** (1×10^{-5} M) in different solvents under ambient (c) and UV light (365 nm) (d).

Table S4 Photophysical data for **SMC-4** in different solvents

Solvents	λ_{ab} (nm)[a]	λ_{em} (nm)[a]	Φ_{fl} (%)[b]	τ (ns)[c]	Stokes shift (cm^{-1})[a]	FWHM (nm)[d]	K_r (10^7 s^{-1})[e]	K_{nr} (10^8 s^{-1})[f]
CH	461	528	21.26	2.78	2752	78.64	7.65	2.83
MCH	461	528	39.21	2.82	2752	62.5	13.90	2.16
Tol	475	582	53.35	7.96	3870	91.69	6.70	0.57
Xyl	475	590	55.24	6.47	4103	108.04	8.54	0.69
$CHCl_3$	486	686	21.98	4.26	5998	127.3	5.16	1.83
THF	477	670	34.04	6.07	6038	144.94	5.61	1.09
EA	475	668	25.6	5.18	6082	142.45	4.94	1.43
DCM	485	712	17.79	4.65	6574	111.56	3.83	1.77

[a]Measured in different solvents (1×10^{-5} M) at 300 K; [b]Absolute fluorescence quantum yield (Φ_{fl}) evaluated using an integrating sphere under air; [c]Fluorescence lifetimes (τ) measured under air at 300 K; [d]Full width at half-maximum (FWHM) of the fluorescence spectrum, given in wavelength; [e]Rate constant of fluorescence radiative decay: $K_r = \Phi_{fl}/\tau$; [f]Rate constant of nonradiative: $K_{nr} = (1 - \Phi_{fl})/\Phi_{fl}$

3.Lippert-MatagaAnalysis

To better evaluate the effects of solvents on the emission features, the relationship between the solvent polarity parameter and the Stokes shift according to the Lippert–Mataga equation was investigated.[2]

$$\Delta v = v_a - v_e = \frac{2(\mu_e - \mu_g)^2}{hca^3}\Delta f + \text{consistant}\text{----------} (1)$$

$$\Delta f = \frac{\varepsilon - 1}{2\varepsilon + 1} - \frac{n^2 - 1}{2n^2 + 1}$$

where Δv stands for the Stokes shift, v_a and v_e represent the maximum absorption and emission wavenumbers (cm^{-1}), respectively. The letter h is Planck's constant, c is the speed of light in a vacuum, a is the Onsager radius. μ_e and μ_g are the permanent dipole moments of the excited state and the ground state, respectively. The letter ε is the static dielectric constant of the solvent, n is the refractive index, and Δf is the orientational polarizability.

Figure S7–S11 show the plots of the Stokes shifts (Δv) versus orientational polarizability (Δf) for **MC-1** and **SMC-1–4**, respectively. According to the Lippert–Mataga equation, the slope of the best-fit line was related to the dipole moment change between the ground state and the excited state ($\Delta\mu = \mu_e - \mu_g$).

Upon simplifying equation (1), we get the following equation:

$\Delta\mu = 0.00487\times(V\times m)^{1/2}$ ---------- (2)

where V is the volume of the fluorophore in $Å^3$ (Volumes were calculated by molecular mechanics in Spartan) and m is the slope of the linear fit obtained upon plotting vs Δf in cm^{-1}, $\Delta\mu$ in debye (D)

Table S5. Molecular volumes (V), slops of the linear fit (m), and dipole moment changes ($\Delta\mu$) of **MC-1** and **SMC-1–4**.

Componds	V (Å^3)	m	$\Delta\mu$ (D)
MC-1	1467	24383	29
SMC-1	677	22352	19
SMC-2	822	23661	21
SMC-3	505	24415	17
SMC-4	505	15936	14

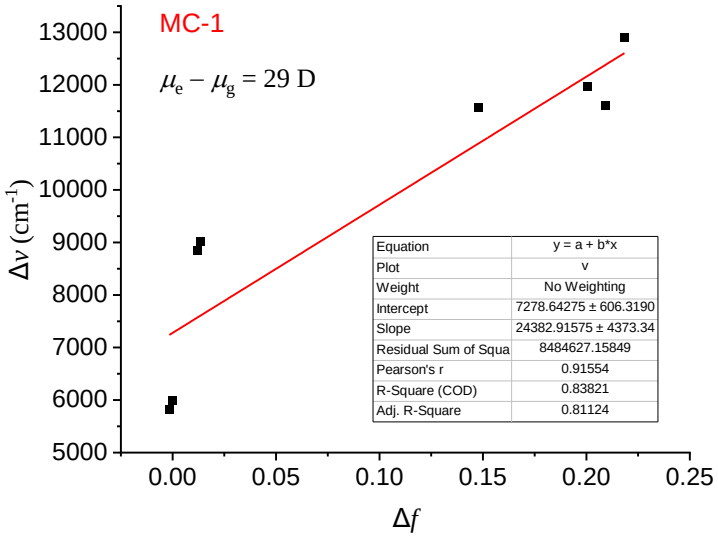

Figure S7. Lippert-Mataga plot of emission maxima of **MC-1** in different solvents against solvent orientation polarizabilities

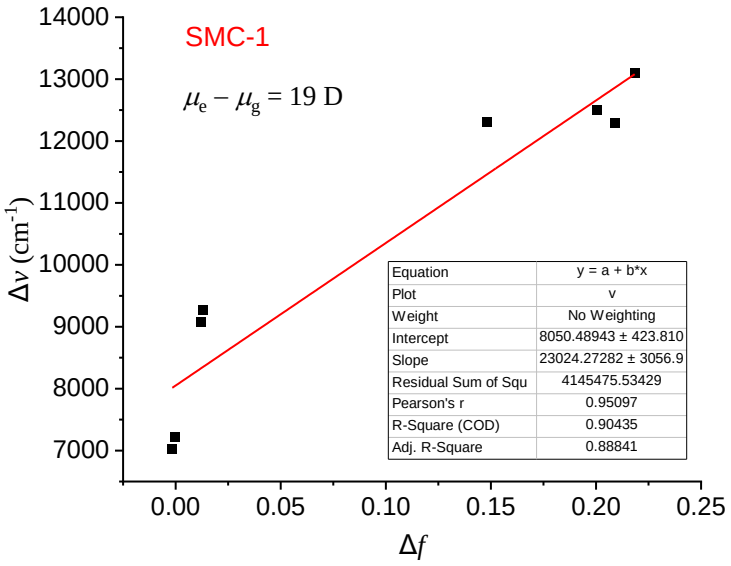

Figure S8. Lippert-Mataga plot of emission maxima of **SMC-1** in different solvents against solvent orientation polarizabilities

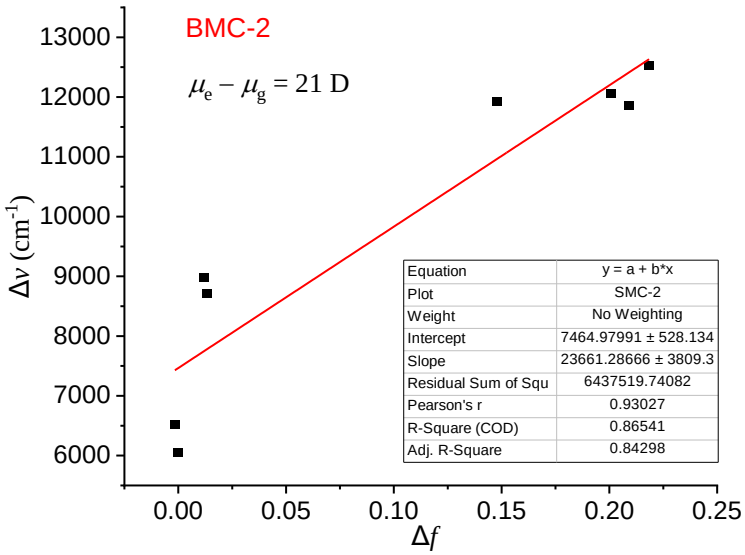

Figure S9. Lippert-Mataga plot of emission maxima of **SMC-2** in different solvents against solvent orientation polarizabilities

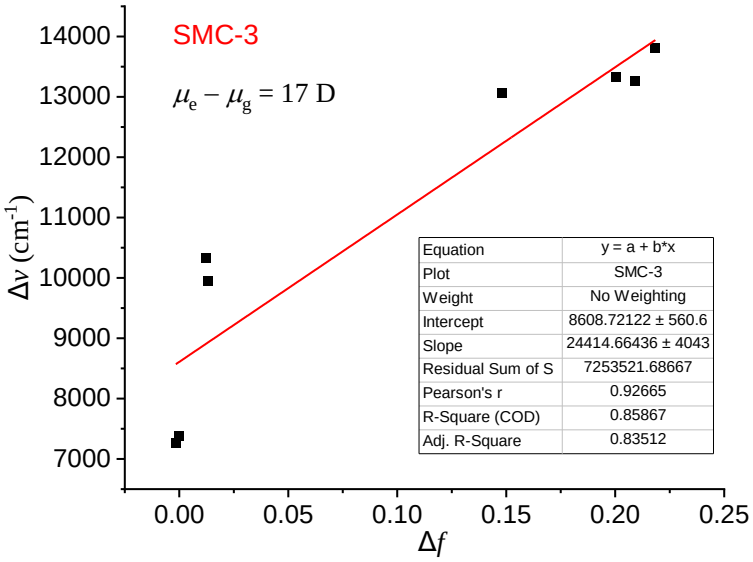

Figure S10. Lippert-Mataga plot of emission maxima of **SMC-3** in different solvents against solvent orientation polarizabilities

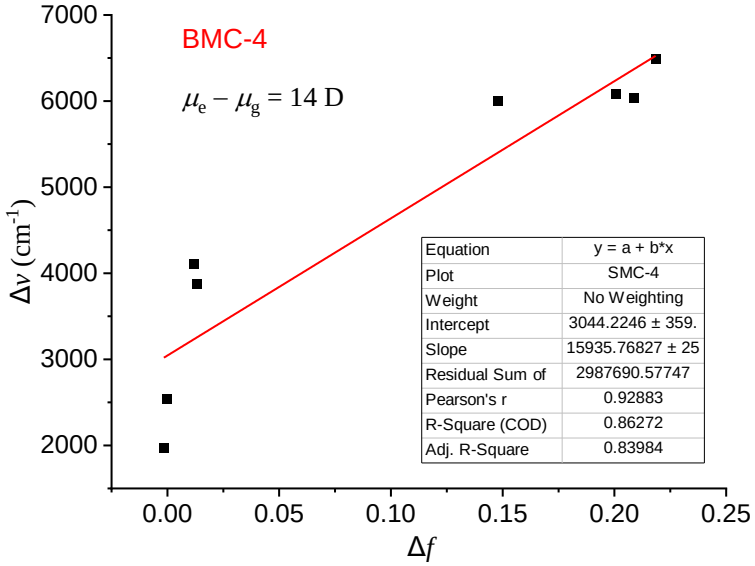

Figure S11. Lippert-Mataga plot of emission maxima of **SMC-4** in different solvents against solvent orientation polarizabilities

4. Theoretical Calculations.

DFT calculations were performed with the Gaussian 09 software package.[3] Geometry optimizations and vertical excitations were calculated by means of hybrid density functional B3LYP with the basis set of 6-31G(d,p). The input files and orbital representations were generated with Gaussview 5.0. Excitation energies and oscillator strengths for the optimized structures were calculated using TD-DFT (B3LYP/6-31G(d,p)). The frontier molecular orbitals of **MC-1** and **SMC-1–4** were calculated using simplified model molecules **MC-1'** and **SMC-1'–4'**, which have smaller methyl groups replacing the *n*-hexyl groups to reduce the computational cost.

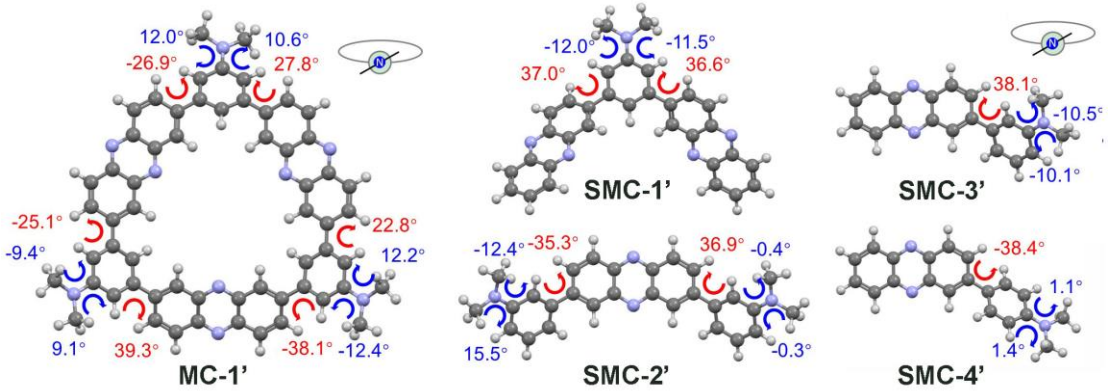

Figure S12. Calculated excited state geometries of **MC-1'** and **SMC-1'–4'** (DFT-B3LYP/6-31G(d,p)) using the simplified models with torsion angles labeled. The *n*-hexyl groups are simplified as methyl groups.

Table S6 Torsion angles of **MC-1'** at ground state and excited state.[a]

C-C single bond			C-N single bond		
Ground state (°)	Excited state (°)	$\Delta\theta$ (°)	Ground state (°)	Excited state (°)	$\Delta\theta$ (°)
-28.9	-26.9	2	-9.9	12.0	**21.9**
28.8	27.8	1	9.2	10.6	1.4
24.3	22.8	1.5	9.2	12.2	3
-38.3	-38.1	0.2	-9.6	-12.4	2.8
38.5	39.3	0.8	9.3	9.1	0.2
-24.5	-25.1	0.6	-9.4	-9.4	0

[a]Torsion angle values were obtained from the optimaized structure of **MC-1'** at ground state and excited state.

Table S7 Torsion angles of **SMC-1'–4'** at ground state and excited state.[a].

	C-C single bond			C-N single bond		
	Ground state (°)	Excited state (°)	$\Delta\theta$ (°)	Ground state (°)	Excited state (°)	$\Delta\theta$ (°)
SMC-1	38.7	37.0	1.7	-1.6	-12.0	**10.4**
	38.7	36.6	2.1	-1.6	-11.5	**9.9**
SMC-2	-37.6	-35.3	2.3	-9.8	-12.4	2.6
				11.7	15.5	3.8
	37.6	36.9	0.7	9.7	-0.4	**10.1**
				-11.7	-0.3	**11.4**
SMC-3	37.7	38.1	0.4	9.6	-10.5	**20.1**
				-11.4	-10.1	1.3
SMC-4	-33.3	-38.4	5.1	-8.1	1.1	**9.2**
				9.5	1.4	**8.1**

[a]Torsion angle values were obtained from the optimaized structure of **MC-1'** at ground state and excited state.

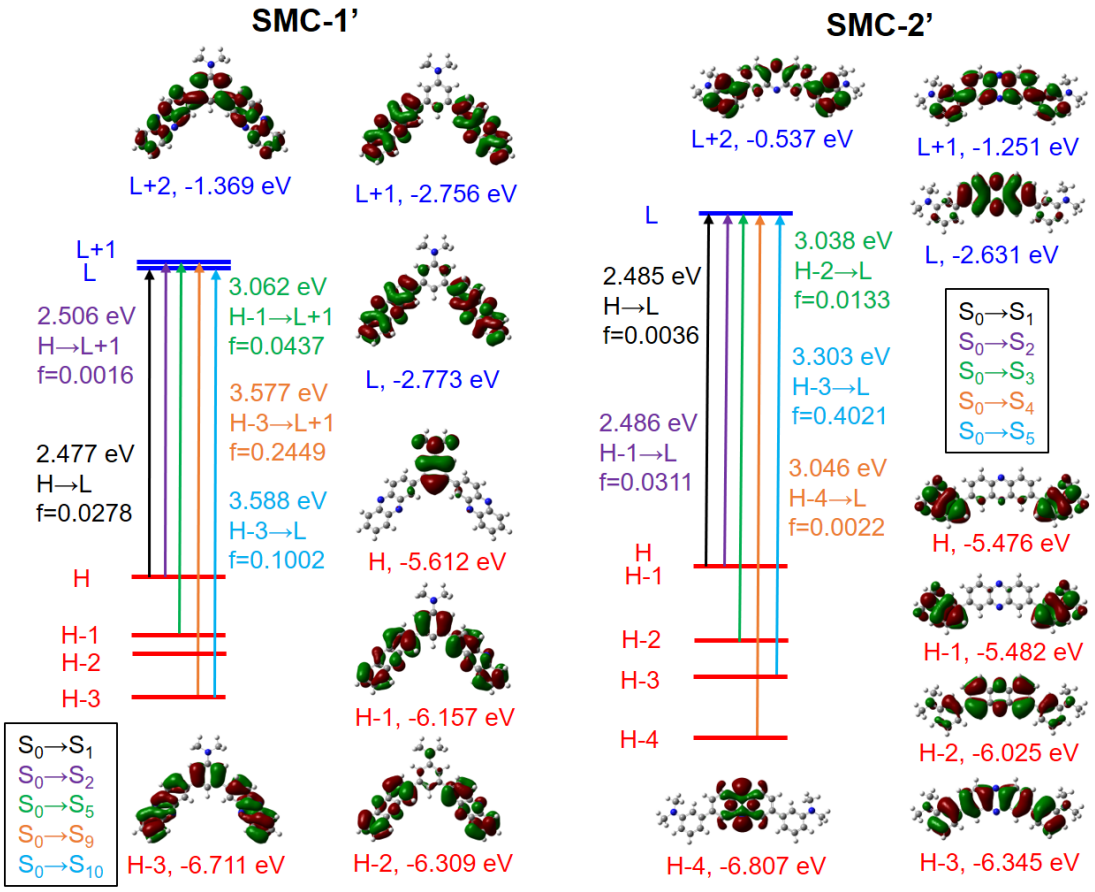

Figure S13. Energy-level diagrams and pictorial representation of frontier molecular orbitals of **SMC-1'** and **SMC-2'** in its optimized ground-state geometry, calculated at the B3LYP/6-31G(d,p) level in gas phase. The *n*-hexyl groups are simplified as methyl groups. H = HOMO; L = LUMO.

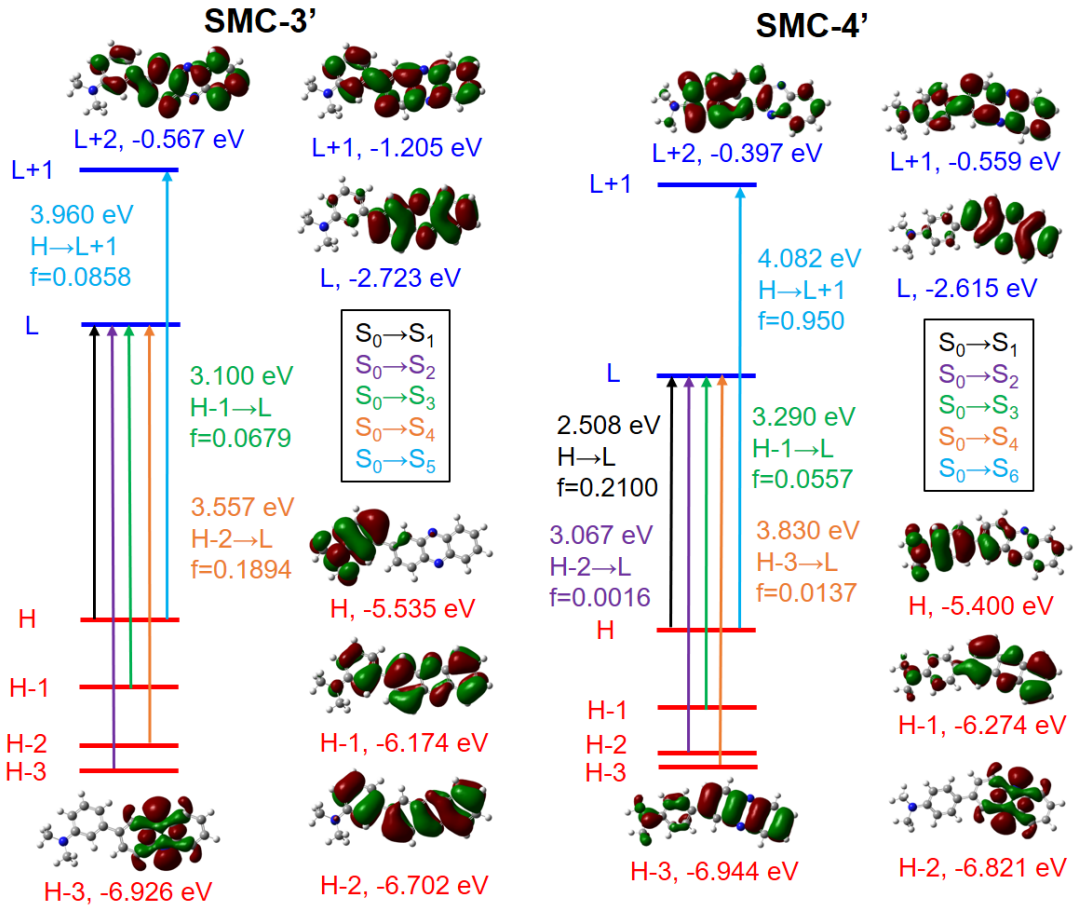

Figure S14. Energy-level diagrams and pictorial representation of frontier molecular orbitals of **SMC-3'** and **SMC-4'** in its optimized ground-state geometry, calculated at the B3LYP/6-31G(d,p) level in gas phase. The *n*-hexyl groups are simplified as methyl groups. H = HOMO; L = LUMO.

Table S8 Computed excitation energies and oscillator strengths for **MC-1** from TD-DFT calculations

State	Excitation energy		Oscillator strength (*f*)	Excitation	Weight
	[eV]	[nm]			
1	2.4821	499.51	0.0004	HOMO-2→LUMO	0.18877
				HOMO-2→LUMO+2	-0.11153
				HOMO-1→LUMO+1	0.22719
				HOMO→LUMO	0.61818
				HOMO→LUMO+2	-0.1257
2	2.4893	498.07	0.0052	HOMO-2→LUMO+1	0.23045
				HOMO-1→LUMO	-0.29357
				HOMO-1→LUMO+2	0.46867
				HOMO→LUMO+1	-0.369
3	2.4896	498.01	0.0028	HOMO-2→LUMO+1	0.40833
				HOMO-1→LUMO	0.13928
				HOMO-1→LUMO+2	0.26591
				HOMO→LUMO+1	0.48693
4	2.4946	497.01	0.0076	HOMO-2→LUMO	-0.16505
				HOMO-2→LUMO+2	-0.40955
				HOMO→LUMO	0.10764
				HOMO→LUMO+2	0.53378
5	2.5005	495.83	0.0118	HOMO-2→LUMO	0.53193

				HOMO-2→LUMO+2	-0.16494
				HOMO-1→LUMO	-0.10993
				HOMO-1→LUMO+1	-0.3895
				HOMO-1→LUMO+2	-0.11879
6	2.501	495.74	0.0113	HOMO-2→LUMO	0.14933
				HOMO-2→LUMO+1	-0.35025
				HOMO-1→LUMO	0.42627
				HOMO-1→LUMO+2	0.39739
7	2.6951	460.03	0.0002	HOMO-2→LUMO	-0.15434
				HOMO-2→LUMO+1	0.32527
				HOMO-1→LUMO	0.39365
				HOMO-1→LUMO+1	-0.25081
				HOMO-1→LUMO+2	-0.17134
				HOMO→LUMO	0.13756
				HOMO→LUMO+1	-0.30201
				HOMO→LUMO+2	-0.1013
8	2.6961	459.86	0.0001	HOMO-2→LUMO	0.30528
				HOMO-2→LUMO+1	0.20204
				HOMO-1→LUMO	0.20696
				HOMO-1→LUMO+1	0.45933
				HOMO→LUMO	-0.22931
				HOMO→LUMO+1	-0.16975
				HOMO→LUMO+2	0.15441
9	2.7013	458.97	0.0000	HOMO-2→LUMO	0.1112
				HOMO-2→LUMO+2	0.53626
				HOMO→LUMO	0.17442
				HOMO→LUMO+2	0.40032
10	2.9442	421.12	0.0018	HOMO-4→LUMO+1	0.16235
				HOMO-3→LUMO	0.64982
				HOMO-3→LUMO+2	-0.15595
11	2.9571	419.28	0.0024	HOMO-4→LUMO	0.51409
				HOMO-4→LUMO+2	0.35273
				HOMO-3→LUMO+1	0.29422
12	2.9841	415.48	0.0046	HOMO-9→LUMO	0.10623
				HOMO-6→LUMO	-0.3431
				HOMO-4→LUMO+1	0.48519
				HOMO-3→LUMO+2	0.31564
13	2.9952	413.94	0.0004	HOMO-4→LUMO+2	0.50447
				HOMO-3→LUMO+1	-0.46672
14	3.0189	410.7	0.0489	HOMO-11→LUMO	0.25721
				HOMO-10→LUMO	-0.27585
				HOMO-10→LUMO+2	0.10344
				HOMO-9→LUMO+1	0.38939
				HOMO-6→LUMO+1	-0.1086
				HOMO-4→LUMO	0.24257
				HOMO-4→LUMO+2	-0.20461
				HOMO-3→LUMO+1	-0.25999
15	3.0267	409.64	0.0080	HOMO-11→LUMO+1	0.29873
				HOMO-10→LUMO+1	-0.32905
				HOMO-9→LUMO	0.43724
				HOMO-9→LUMO+2	-0.14729
				HOMO-3→LUMO+2	-0.26808
16	3.0312	409.03	0.0020	HOMO-11→LUMO	0.16488
				HOMO-11→LUMO+2	0.48808
				HOMO-10→LUMO	0.17907
				HOMO-10→LUMO+2	0.43551

17	3.0395	407.9	0.0652	HOMO-11→LUMO HOMO-10→LUMO HOMO-9→LUMO+1 HOMO-4→LUMO HOMO-4→LUMO+2 HOMO-3→LUMO+1	-0.20123 0.20191 -0.29269 0.37721 -0.24244 -0.32693
18	3.0425	407.5	0.0773	HOMO-11→LUMO+1 HOMO-10→LUMO+1 HOMO-9→LUMO HOMO-6→LUMO+2 HOMO-4→LUMO+1 HOMO-3→LUMO HOMO-3→LUMO+2	0.10709 -0.11802 0.15741 -0.11309 -0.38603 0.21716 0.4805
19	3.1596	392.4	0.0043	HOMO-7→LUMO+1 HOMO-6→LUMO HOMO-4→LUMO+1 HOMO-3→LUMO+2	-0.10585 0.56423 0.28353 0.23949
20	3.2025	387.14	0.0003	HOMO-5→LUMO	0.68987
21	3.2199	385.05	0.0789	HOMO-6→LUMO+1 HOMO-5→LUMO+2	0.2629 0.62977
22	3.2209	384.94	0.0585	HOMO-6→LUMO+2 HOMO-5→LUMO+1	-0.20328 0.65988
23	3.2285	384.03	**0.1816**	HOMO-6→LUMO+1 HOMO-5→LUMO+2 HOMO-4→LUMO	0.59826 -0.28257 0.13976
24	3.2322	383.59	**0.1750**	HOMO-6→LUMO HOMO-6→LUMO+2 HOMO-5→LUMO+1 HOMO-3→LUMO	-0.11734 0.62271 0.21165 0.11731
25	3.5597	348.3	0.0622	HOMO-8→LUMO+1 HOMO-7→LUMO HOMO-7→LUMO+2 HOMO-6→LUMO+1 HOMO-3→LUMO+3 HOMO-1→LUMO+3 HOMO→LUMO+4	-0.13199 0.60912 -0.13129 0.1684 -0.1312 -0.10247 -0.10476

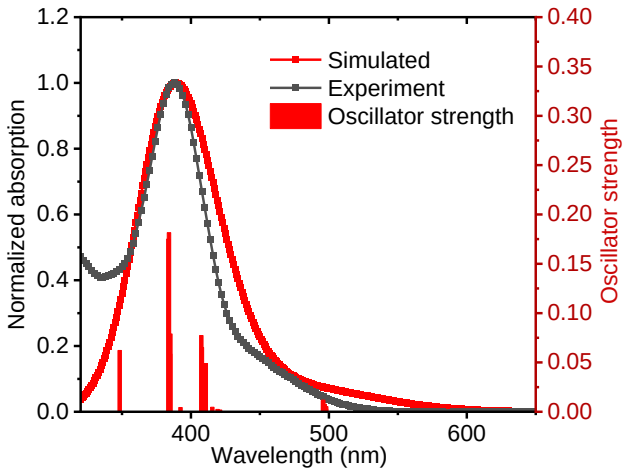

Figure. S15 Experimental UV-vis absorption spectrum in DCM solution (black line) and simulated spectrum (red line) of **MC-1**. Spectra were normalized at the intensity of the lowest energy absorption maxima.

Table S9 Computed excitation energies and oscillator strengths for **SMC-1'** from TD-DFT calculations

State	Excitation energy		Oscillator strength (*f*)	Excitation	Weight
	[eV]	[nm]			
1	2.4772	500.51	0.0278	HOMO→LUMO	0.70540
2	2.5064	494.67	0.0016	HOMO→LUMO+1	0.70562
3	3.051	406.38	0.0080	HOMO-5→LUMO+1 HOMO-4→LUMO HOMO-1→LUMO+1	-0.41116 0.41796 -0.37452
4	3.054	405.97	0.0036	HOMO-5→LUMO HOMO-4→LUMO+1	0.49556 -0.49162
5	3.0618	404.94	0.0437	HOMO-5→LUMO+1 HOMO-4→LUMO HOMO-2→LUMO HOMO-1→LUMO+1	-0.27224 0.27395 -0.12904 0.5708
6	3.082	402.28	0.0730	HOMO-2→LUMO+1 HOMO-1→LUMO	-0.15835 0.67819
7	3.2356	383.19	0.0233	HOMO-2→LUMO HOMO-1→LUMO+1	0.68119 0.14980
8	3.2551	380.89	0.0006	HOMO-2→LUMO+1 HOMO-1→LUMO	0.68096 0.16394
9	3.5774	346.58	0.2449	HOMO-6→LUMO HOMO-3→LUMO+1 HOMO-2→LUMO+2 HOMO-1→LUMO+3	0.19038 0.64017 0.12097 0.11125
10	3.5883	345.52	0.1002	HOMO-6→LUMO+1 HOMO-3→LUMO HOMO-2→LUMO+3 HOMO-1→LUMO+2	0.15635 0.64 -0.13358 -0.17409

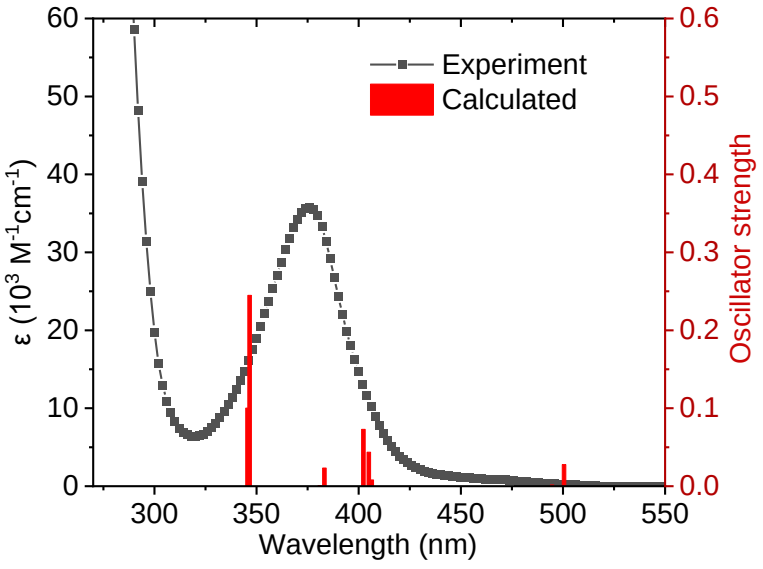

Figure S16. Experimental UV-vis absorption spectrum in DCM solution and oscillator strengths of **SMC-1**

Table S10. Computed excitation energies and oscillator strengths for **SMC-2'** from TD-DFT calculations

State	Excitation energy		Oscillator strength (*f*)	Excitation	Weight
	[eV]	[nm]			
1	2.4848	498.97	0.0036	HOMO-1→LUMO HOMO→LUMO	-0.12673 0.69381
2	2.4859	498.76	0.0311	HOMO-1→LUMO HOMO→LUMO	0.69417 0.12663
3	3.0384	408.06	0.0133	HOMO-4→LUMO HOMO-2→LUMO	0.15833 0.68257
4	3.046	407.04	0.0022	HOMO-4→LUMO HOMO-2→LUMO	0.68432 -0.15713
5	3.303	375.37	0.4021	HOMO-3→LUMO HOMO-2→LUMO+1	0.67757 0.16555
6	3.8821	319.37	0.1538	HOMO-6→LUMO HOMO→LUMO+1	-0.14335 0.67339
7	3.8884	318.86	0.0165	HOMO-5→LUMO HOMO-1→LUMO+1 HOMO→LUMO+2	-0.29085 0.62818 -0.10225
8	3.9771	311.75	0.0059	HOMO-6→LUMO HOMO-2→LUMO+1 HOMO-2→LUMO+3 HOMO→LUMO+1	0.61229 0.26059 0.1156 0.14532
9	3.9817	311.39	0.0400	HOMO-5→LUMO HOMO-1→LUMO+1	0.63088 0.28897
10	4.301	288.27	0.3985	HOMO-7→LUMO HOMO-3→LUMO HOMO-2→LUMO+1	0.5659 -0.11056 0.37194

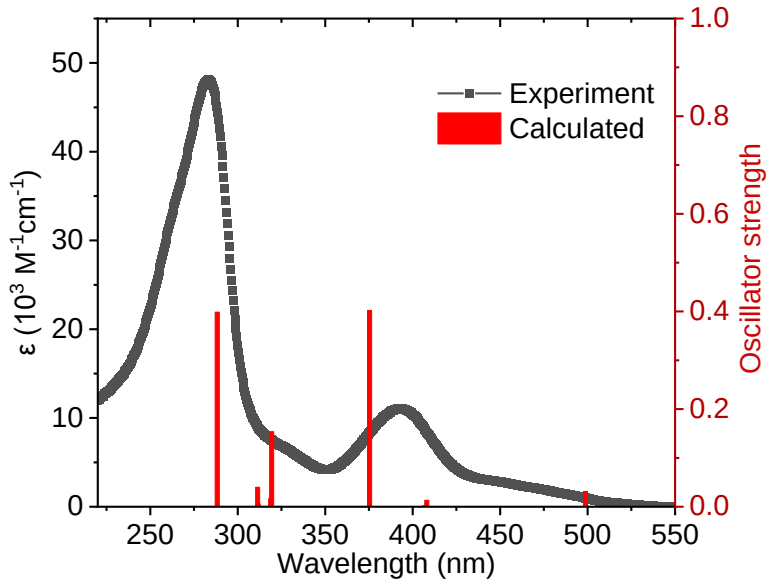

Figure S17. Experimental UV-vis absorption spectrum in DCM solution and oscillator strengths of **SMC-2**

Table S11. Computed excitation energies and oscillator strengths for **SMC-3'** from TD-DFT calculations

State	Excitation energy		Oscillator strength (*f*)	Excitation	Weight
	[eV]	[nm]			
1	2.454	505.23	0.0146	HOMO→LUMO	0.70555
2	3.0581	405.42	0.0023	HOMO-3→LUMO	0.69754
3	3.0995	400.01	0.0679	HOMO-1→LUMO	0.69610
4	3.5568	348.59	0.1894	HOMO-2→LUMO HOMO-1→LUMO+1	0.66056 -0.20322
5	3.9598	313.11	0.0858	HOMO→LUMO+1	0.68674
6	4.003	309.73	0.0119	HOMO-5→LUMO HOMO-4→LUMO HOMO-1→LUMO+1 HOMO-1→LUMO+2	-0.17141 0.62568 0.21038 0.11363
7	4.2558	291.33	0.0253	HOMO-5→LUMO HOMO-4→LUMO HOMO-1→LUMO+1	0.65514 0.11142 0.17024
8	4.6334	267.59	0.0114	HOMO→LUMO+2 HOMO→LUMO+3	0.66532 0.15658
9	4.6832	264.74	0.0026	HOMO-7→LUMO HOMO-3→LUMO+1	0.62946 0.305
10	4.7102	263.22	0.0449	HOMO-7→LUMO HOMO-3→LUMO+1 HOMO-3→LUMO+2 HOMO-1→LUMO+1	-0.30871 0.59183 0.11215 0.11781

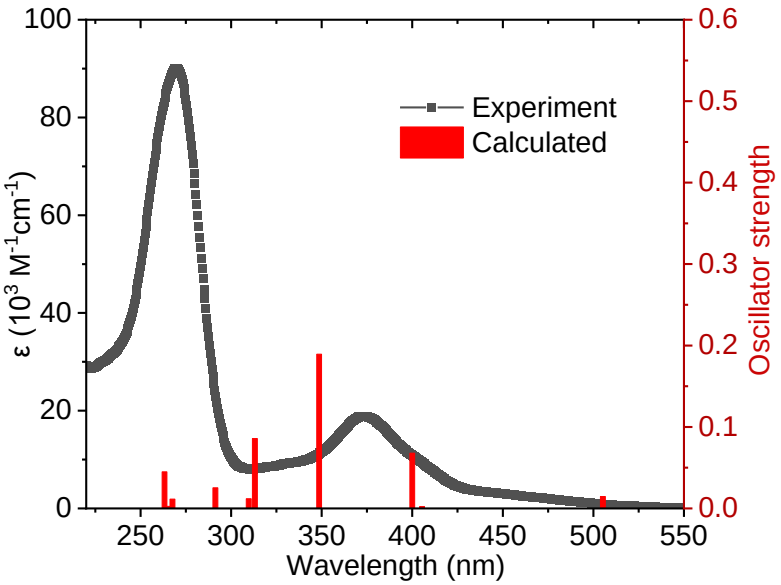

Figure S18. Experimental UV-vis absorption spectrum in DCM solution and oscillator strengths of **SMC-3**

Table S12. Computed excitation energies and oscillator strengths for **SMC-4'** from TD-DFT calculations

State	Excitation energy		Oscillator strength (*f*)	Excitation	Weight
	[eV]	[nm]			
1	2.508	494.36	0.2100	HOMO→LUMO	0.70331
2	3.0672	404.23	0.0016	HOMO-2→LUMO	0.70313
3	3.2904	376.8	0.0557	HOMO-1→LUMO	0.69395
4	3.8303	323.69	0.0137	HOMO-3→LUMO HOMO-1→LUMO+1 HOMO→LUMO+1	0.55008 0.25877 0.32653
5	4.0341	307.34	0.0124	HOMO-4→LUMO HOMO→LUMO+2	0.67861 0.10224
6	4.0815	303.77	0.9496	HOMO-3→LUMO HOMO-1→LUMO+1 HOMO→LUMO+1	-0.29203 -0.13437 0.61087
7	4.1061	301.95	0.0001	HOMO-5→LUMO HOMO-4→LUMO	0.67772 0.10685
8	4.4551	278.29	0.0286	HOMO-4→LUMO HOMO-4→LUMO+1 HOMO→LUMO+2 HOMO→LUMO+3	-0.13132 0.13763 0.59265 -0.29824
9	4.6925	264.22	0.0003	HOMO-7→LUMO HOMO-2→LUMO+1	0.64675 0.27288
10	4.7151	262.95	0.1168	HOMO-2→LUMO+1 HOMO-1→LUMO+1 HOMO→LUMO+2 HOMO→LUMO+3	0.23348 -0.18887 0.2733 0.54015

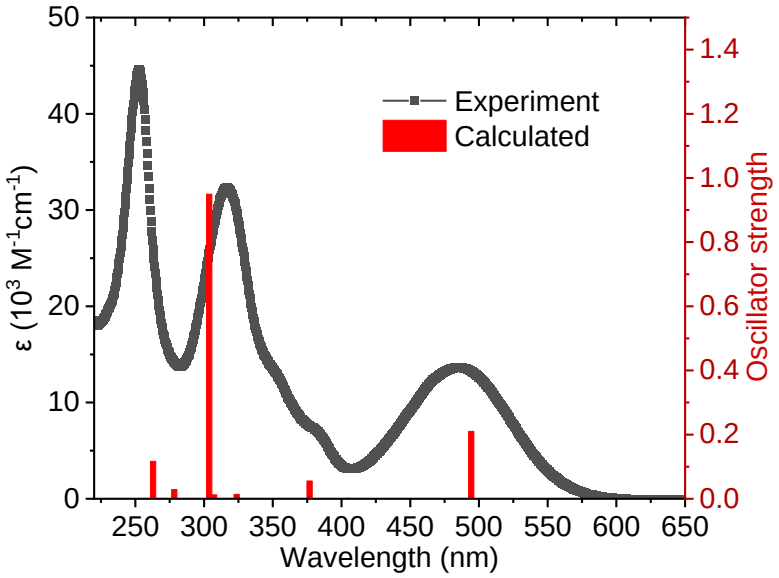

Figure S19. Experimental UV-vis absorption spectrum in DCM solution and oscillator strengths of **SMC-4**

5. Sensing properties

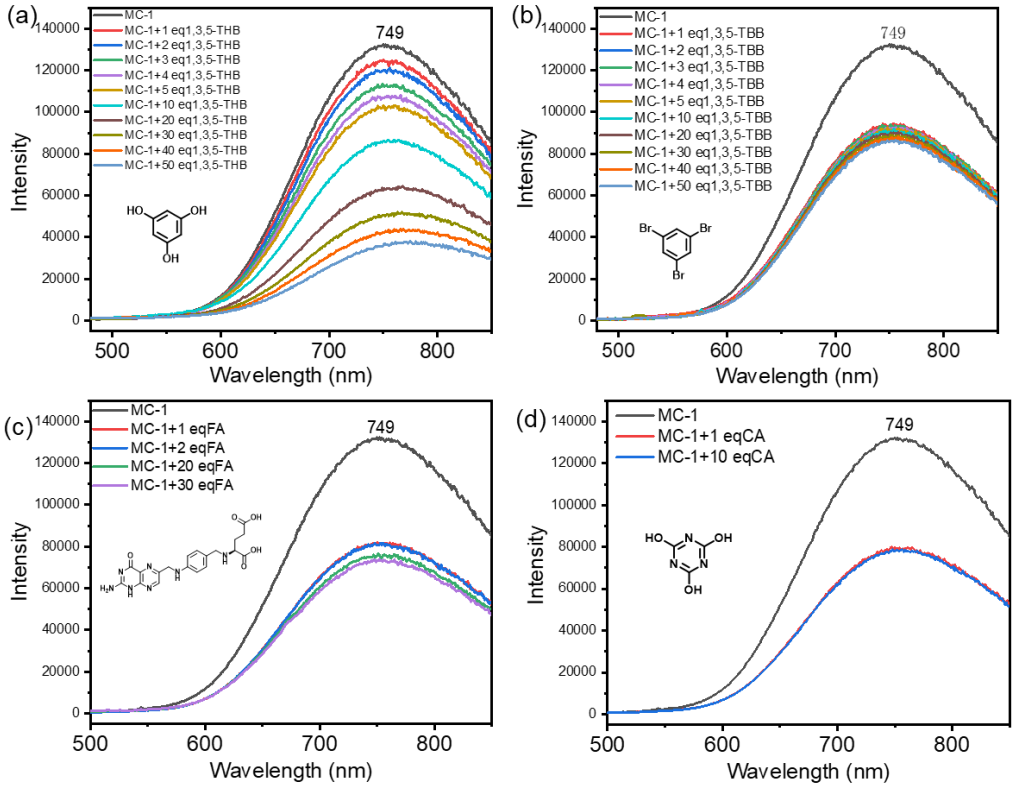

Figure S20. PL spectrum changes of **MC-1** (1×10^{-5} M) when different amounts of (a) phloroglucinol (THB), (b) 1,3,5-tribromobenzene (TBB), (c) folic acid (FA), and (d) cyanuric acid (CA) are added.

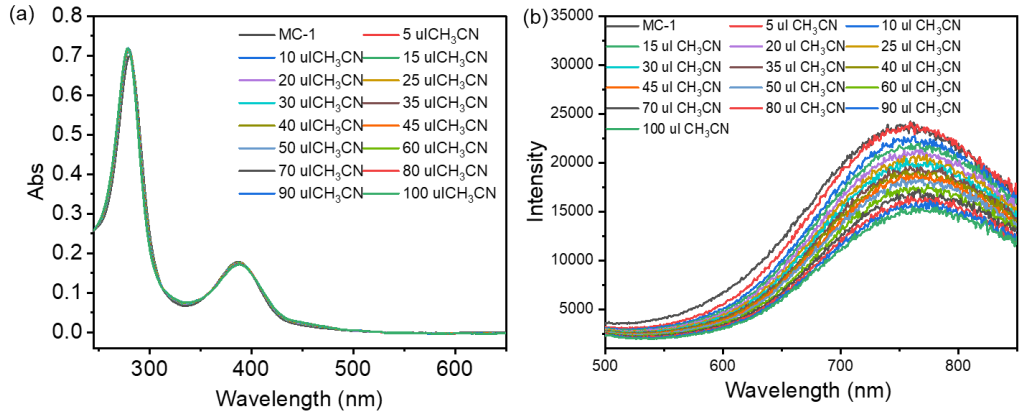

Figure S21. (a) Absorption and (b) emission spectra of **MC-1** in DCM (1×10^{-5} M) recorded when different amounts of acetonitrile (CH_3CN) were added.

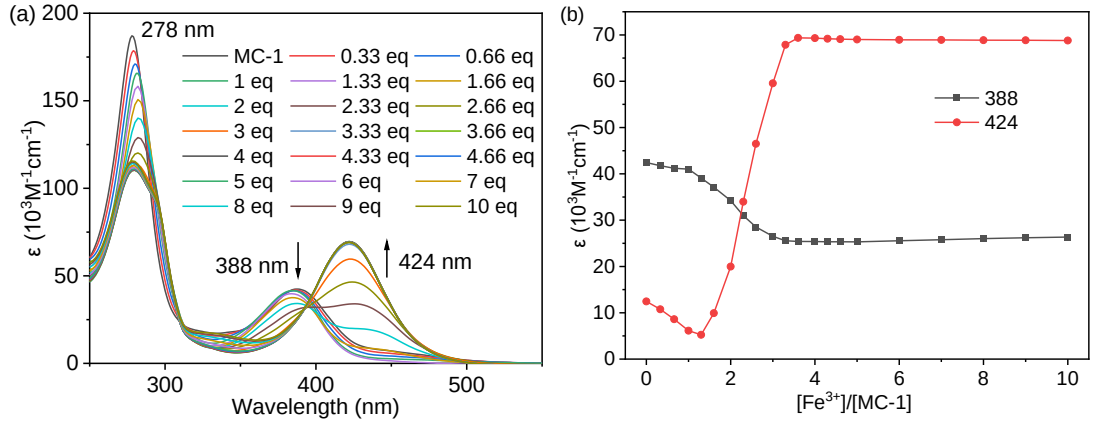

Figure S22. (a) Absorption spectra of **MC-1** in DCM (1×10^{-5} M) with different equivalents of Fe^{3+}. (b) Molar extinction coefficient (ε) of **MC-1** solution versus different Fe^{3+} equivalents at 388 nm and 424 nm.[4]

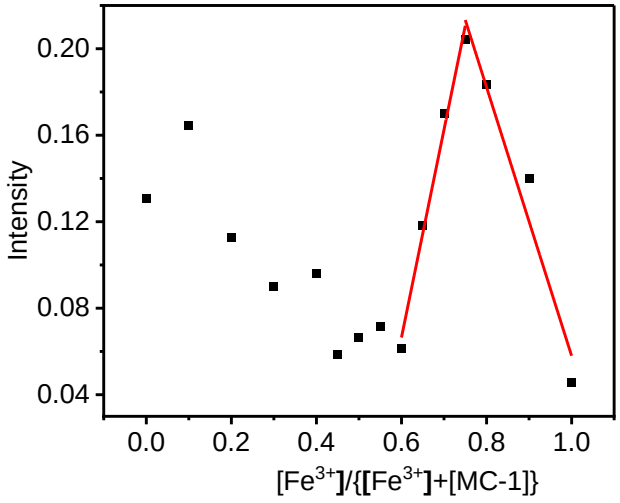

Figure S23. Job's plot of fluorescence intensity of **MC-1** at 545 nm versus the mole fraction of Fe^{3+} ion. The largest fluorescence intensity appeared at the mole fraction of 0.75, indicating that the ratio of **MC-1** to Fe^{3+} is 1:3.

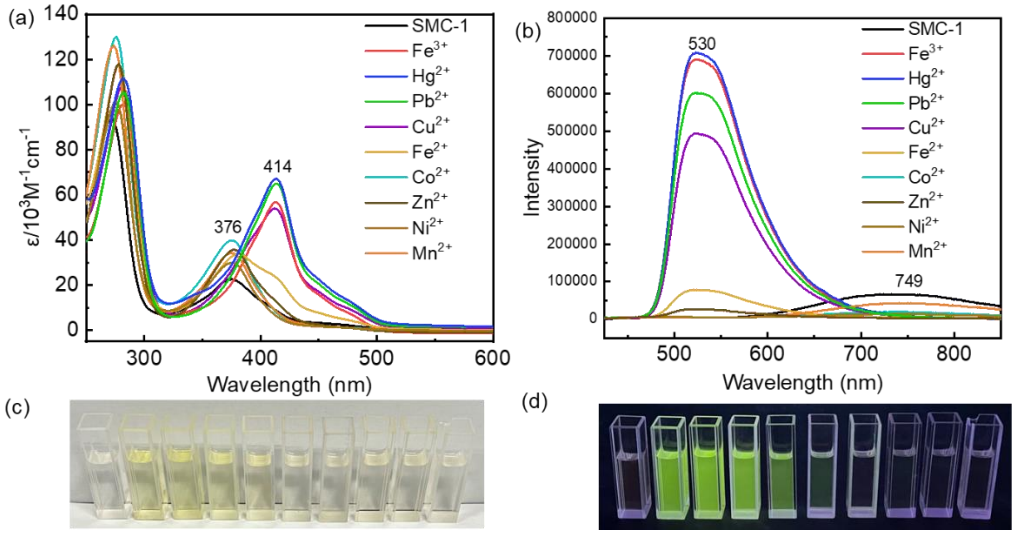

Figure S24. (a) Absorption and (b) emission spectra of **SMC-1** in DCM (1×10^{-5} M) with various metal ions (5 equivalents). (c,d) Images of solutions of **SMC-1** (1×10^{-5} M) with various metal ions under ambient (c) and UV light (365 nm) (d).

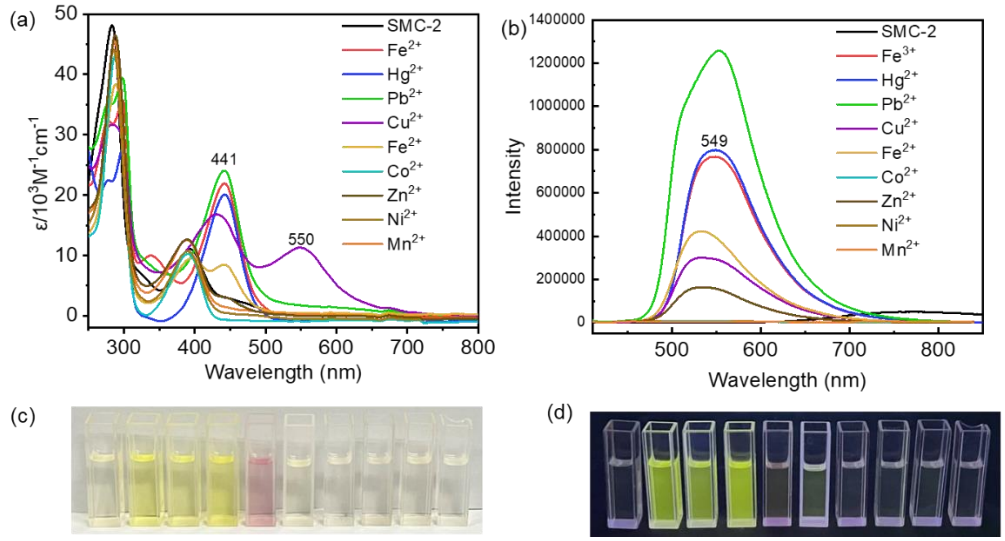

Figure S25. (a) Absorption and (b) emission spectra of **SMC-2** in DCM (1×10^{-5} M) with various metal ions (5 equivalents). (c,d) Images of solutions of **SMC-2** (1×10^{-5} M) with various metal ions under ambient (c) and UV light (365 nm) (d).

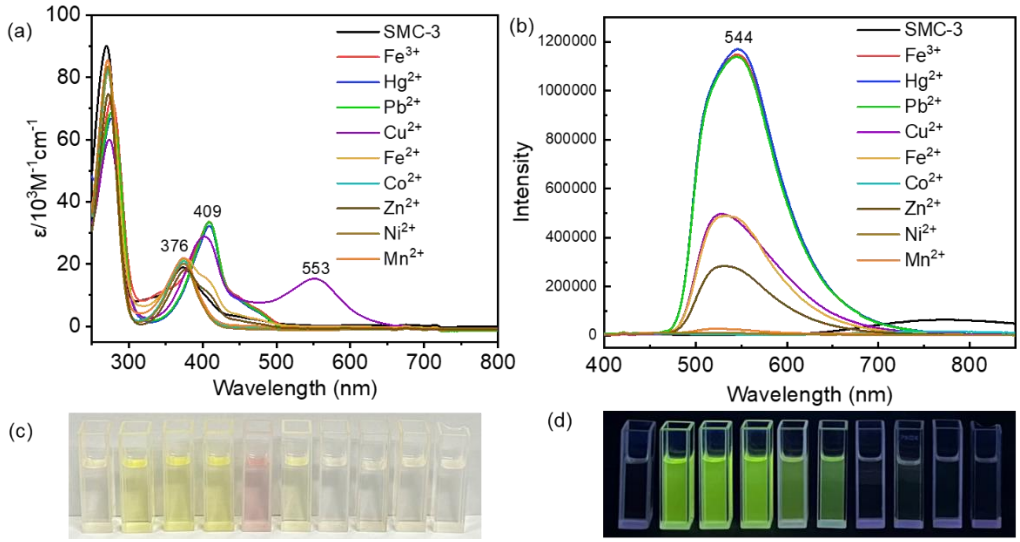

Figure S26. (a) Absorption and (b) emission spectra of **SMC-3** in DCM (1×10^{-5} M) with various metal ions (5 equivalents). (c,d) Images of solutions of **SMC-3** (1×10^{-5} M) with various metal ions under ambient (c) and UV light (365 nm) (d).

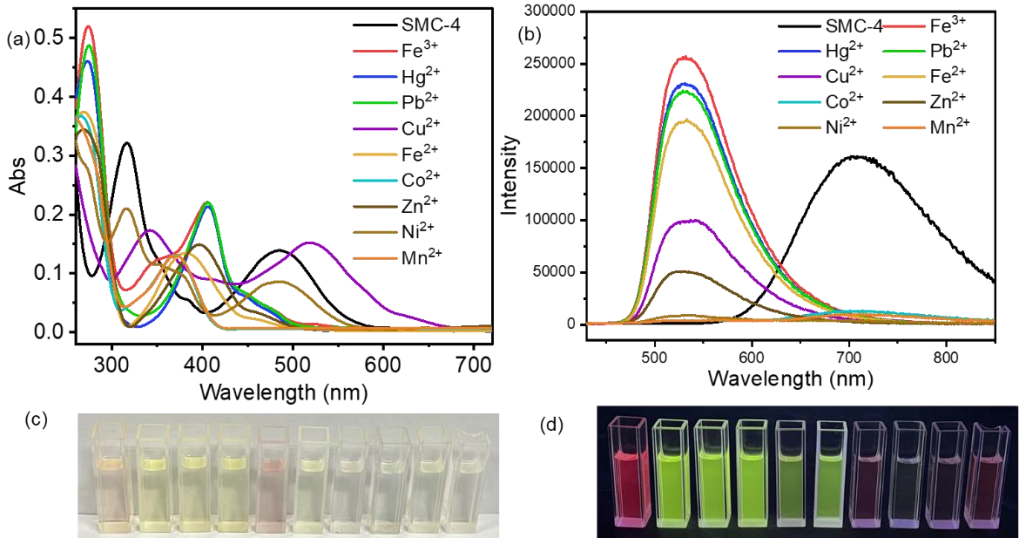

Figure S27. (a) Absorption and (b) emission spectra of **SMC-4** in DCM (1×10^{-5} M) with various metal ions (5 equivalents). (c,d) Images of solutions of **SMC-4** (1×10^{-5} M) with various metal ions under ambient (c) and UV light (365 nm) (d).

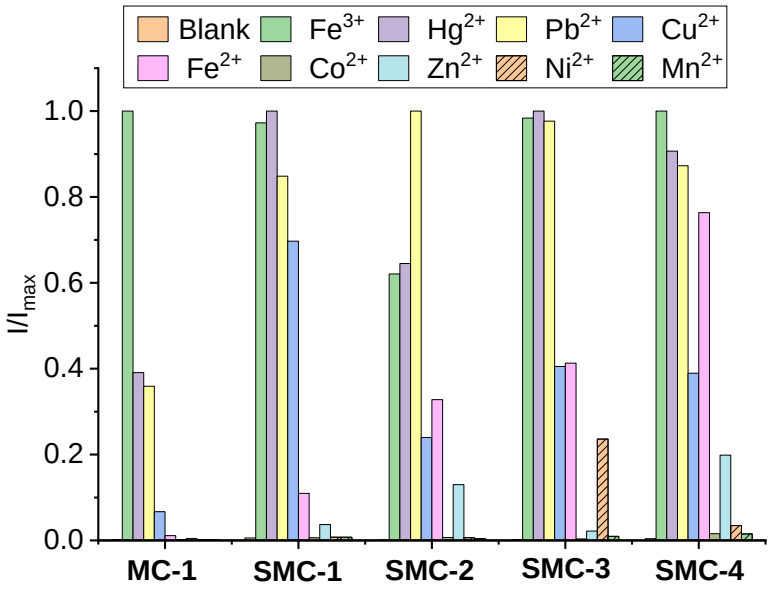

Figure S28. Comparison of normalized fluorescence intensity of **MC-1** and **SMC-1–4** in DCM (1×10^{-5} M) at the most enhanced wavelengths (545, 523, 545, 544, and 531 nm, respectively) with various metal ions (5 equivalents). **MC-1** shows a better selectivity.

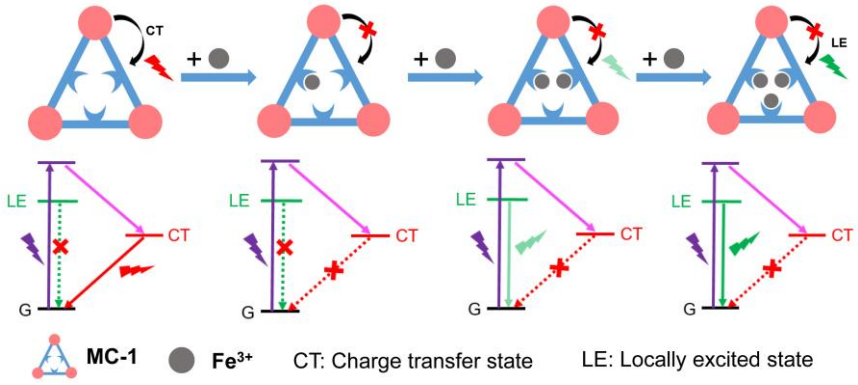

Figure S29. Schematic diagram of the proposed mechanism of **MC-1** recognizing Fe^{3+} ion and the corresponding excited state decay pathway.

6. ^{1}H and ^{13}C-NMR spectra

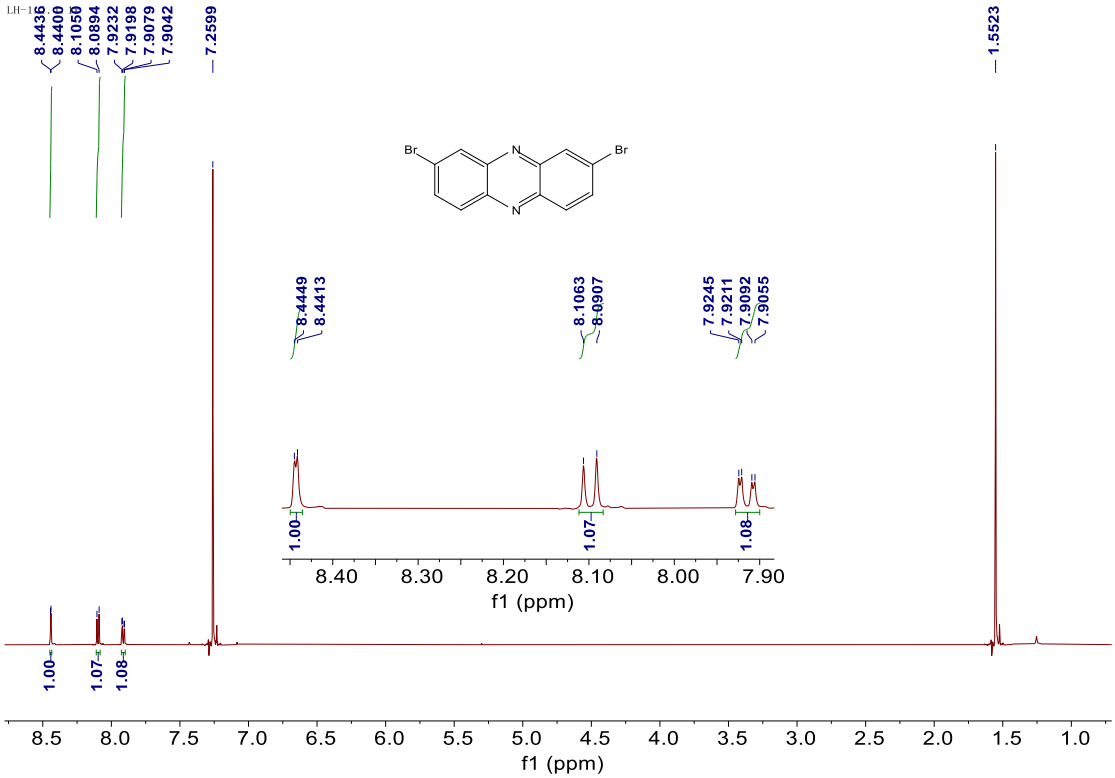

Figure S30. ^{1}H-NMR spectrum of LH-1 in $CDCl_3$

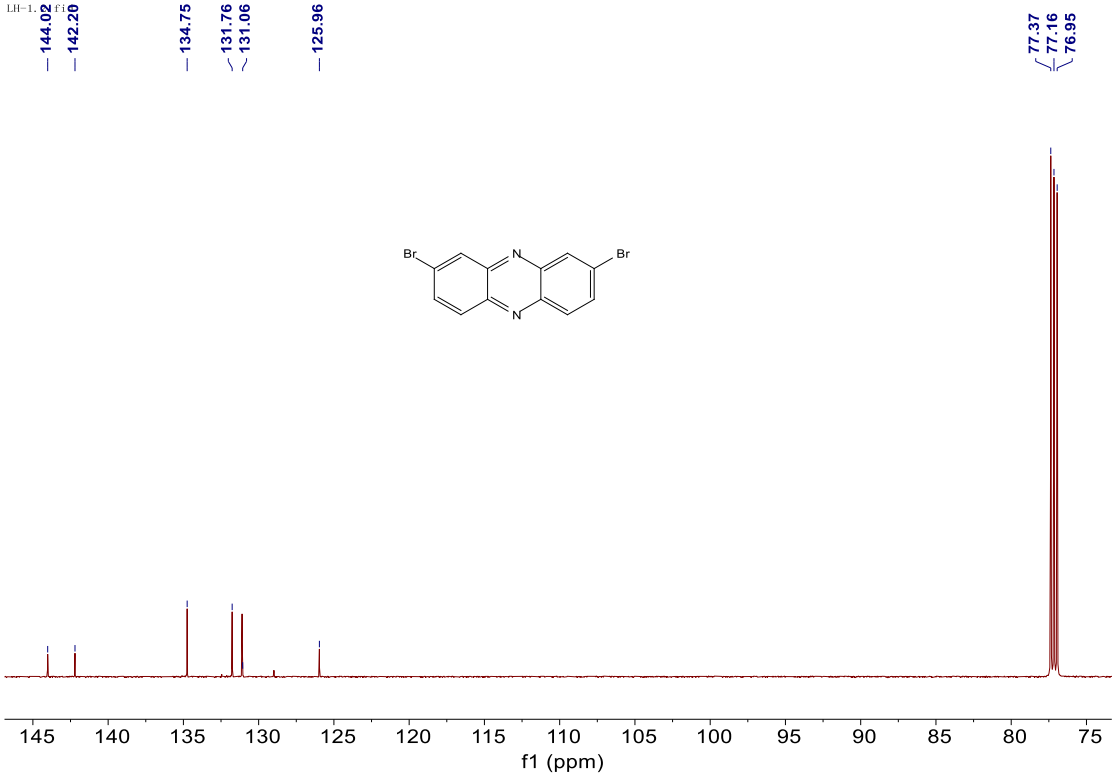

Figure S31. ^{13}C-NMR spectrum of LH-1 in $CDCl_3$

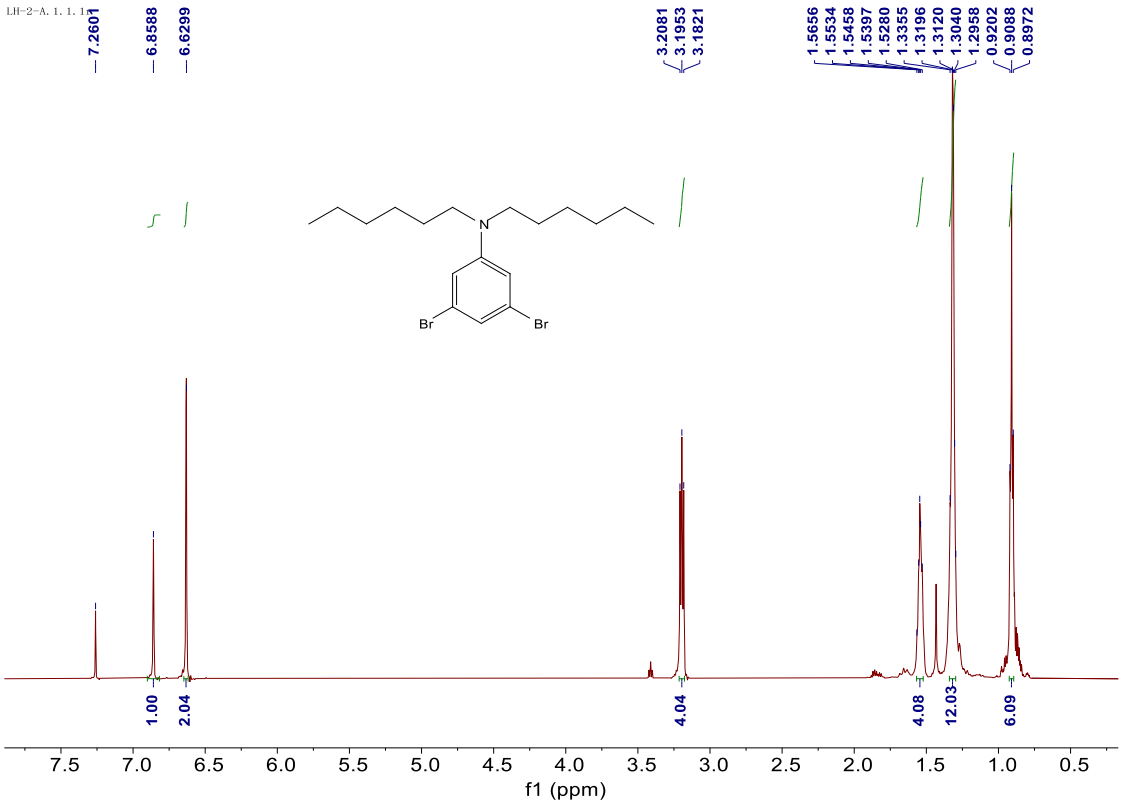

Figure S32. ^{1}H-NMR spectrum of **LH-2** in $CDCl_3$

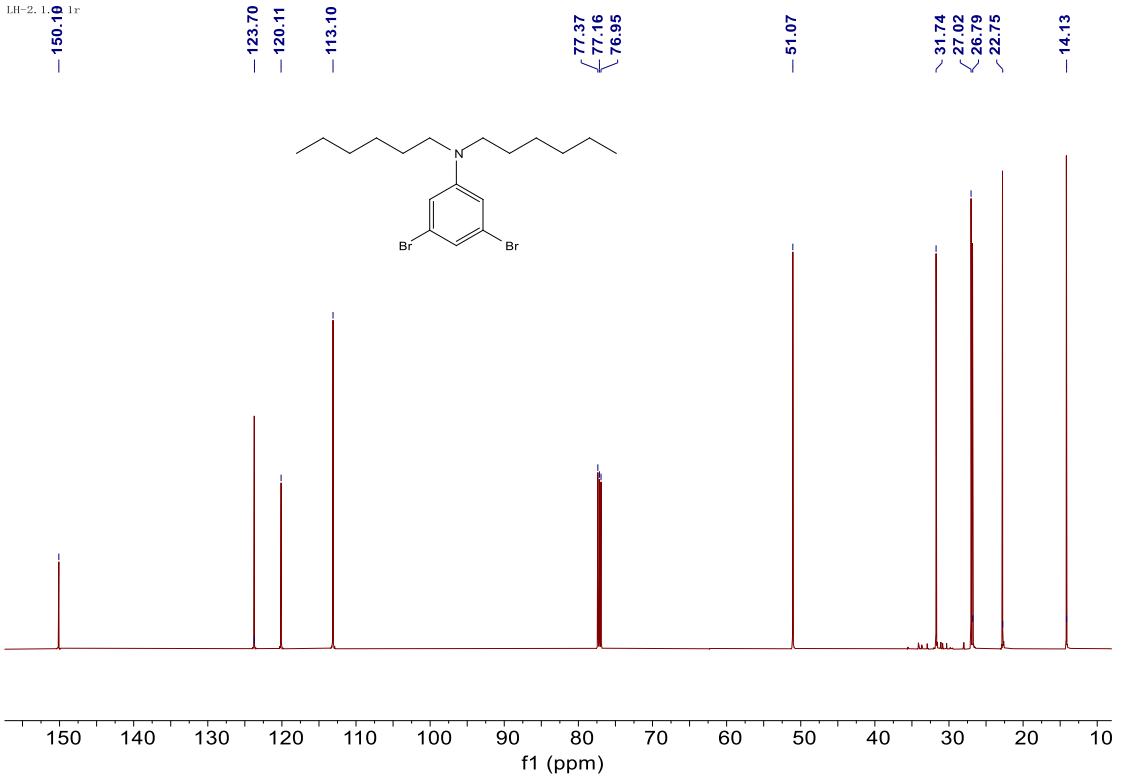

Figure S33. ^{13}C-NMR spectrum of **LH-2** in $CDCl_3$

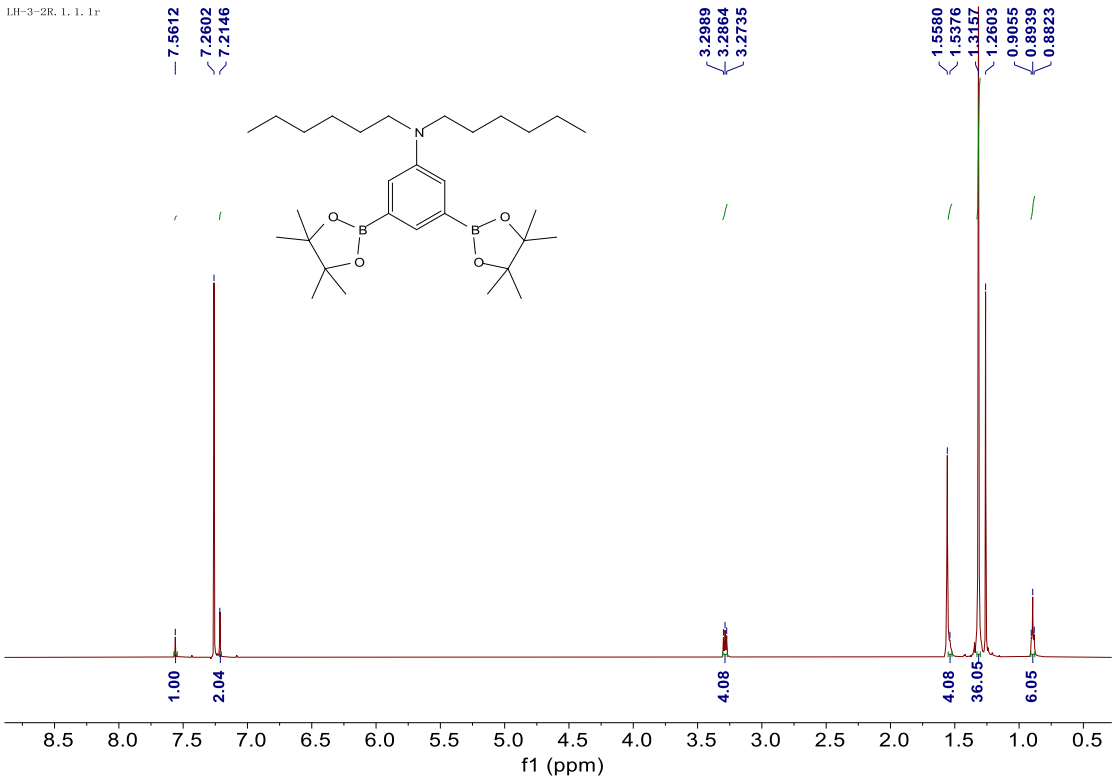

Figure S34. ^{1}H-NMR spectrum of **LH-3** in $CDCl_3$

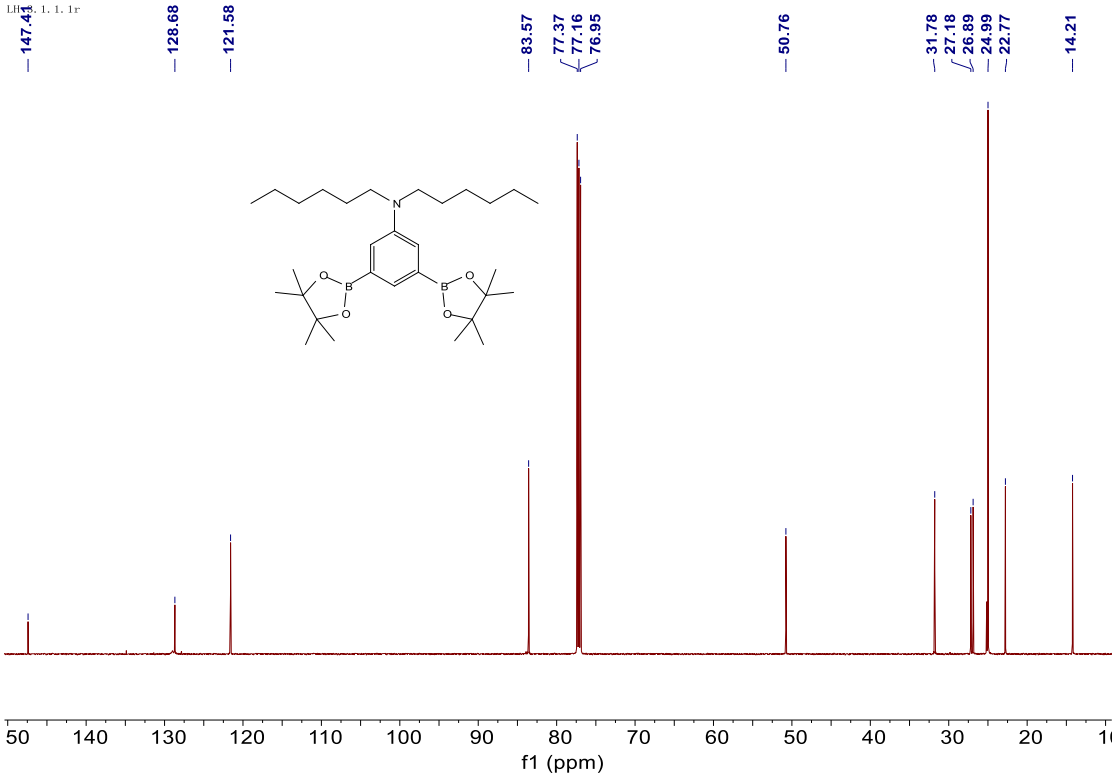

Figure S35. ^{13}C-NMR spectrum of **LH-3** in $CDCl_3$

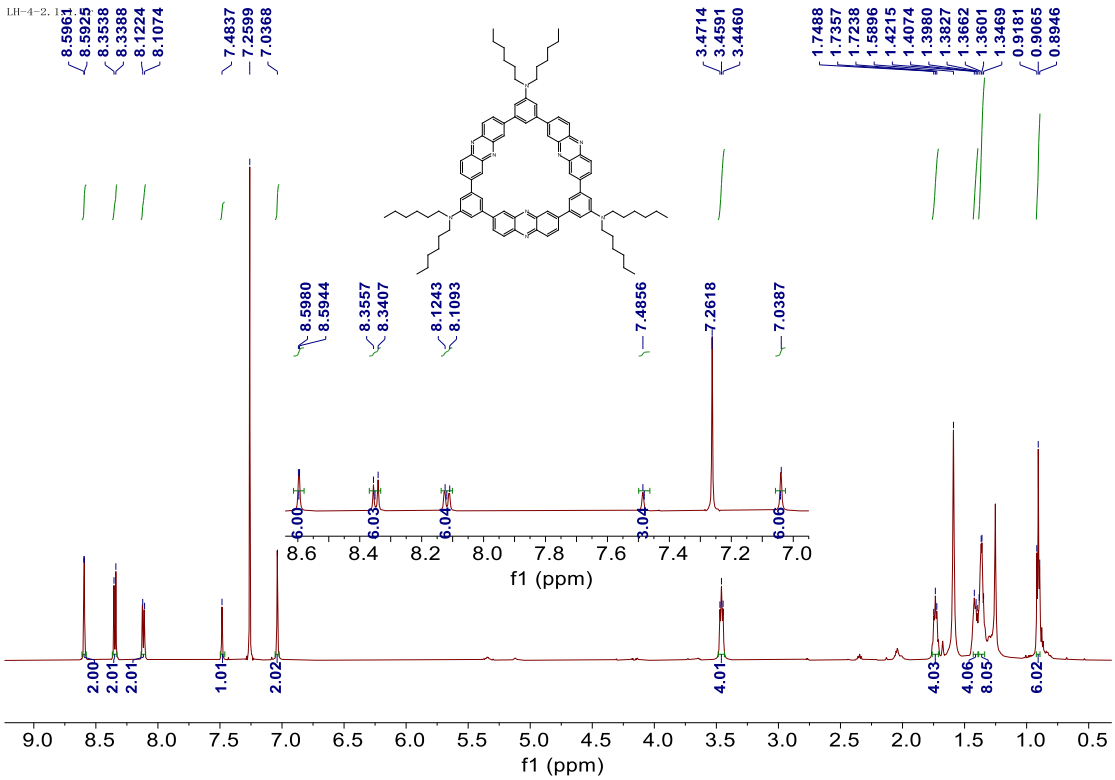

Figure S36. ^{1}H-NMR spectrum of **MC-1** in $CDCl_3$

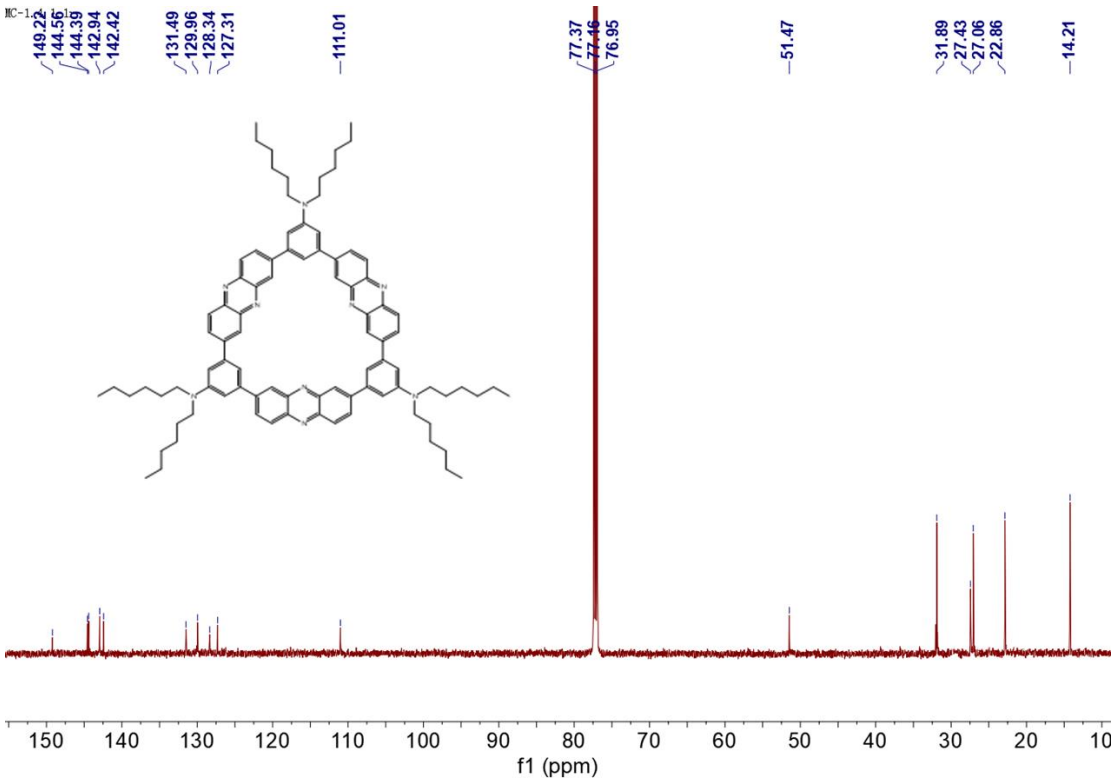

Figure S37. ^{13}C-NMR spectrum of **MC-1** in $CDCl_3$

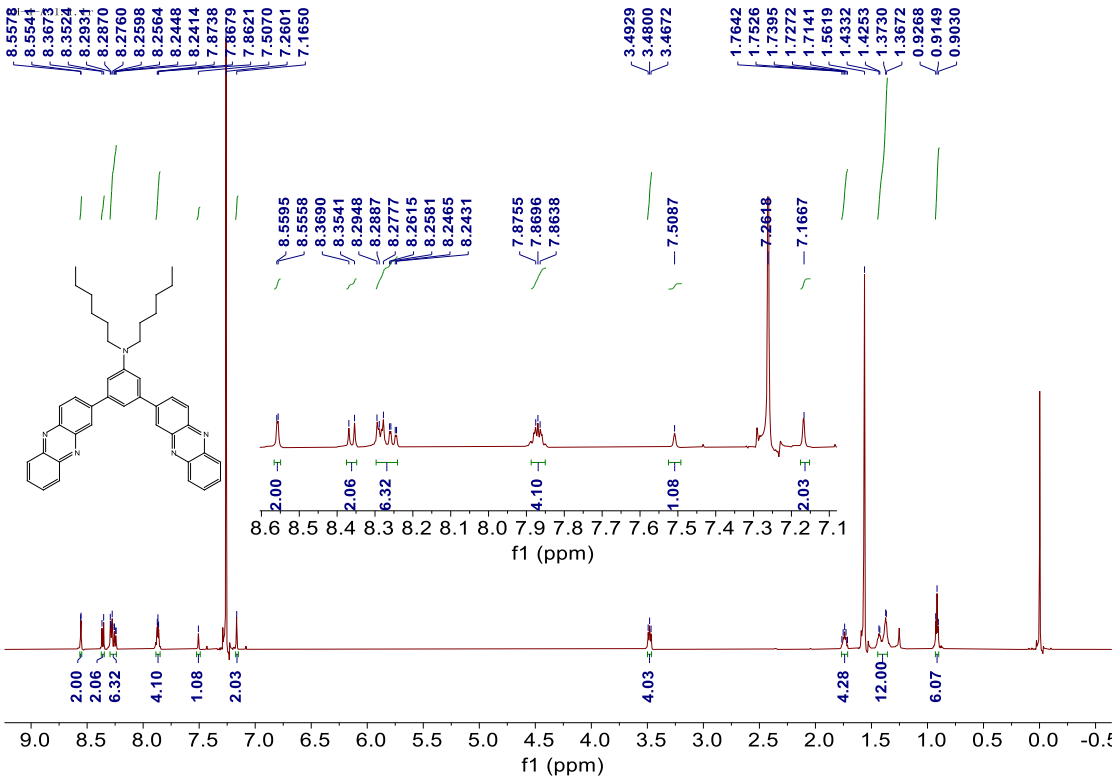

Figure S38. ^{1}H-NMR spectrum of **SMC-1** in $CDCl_3$

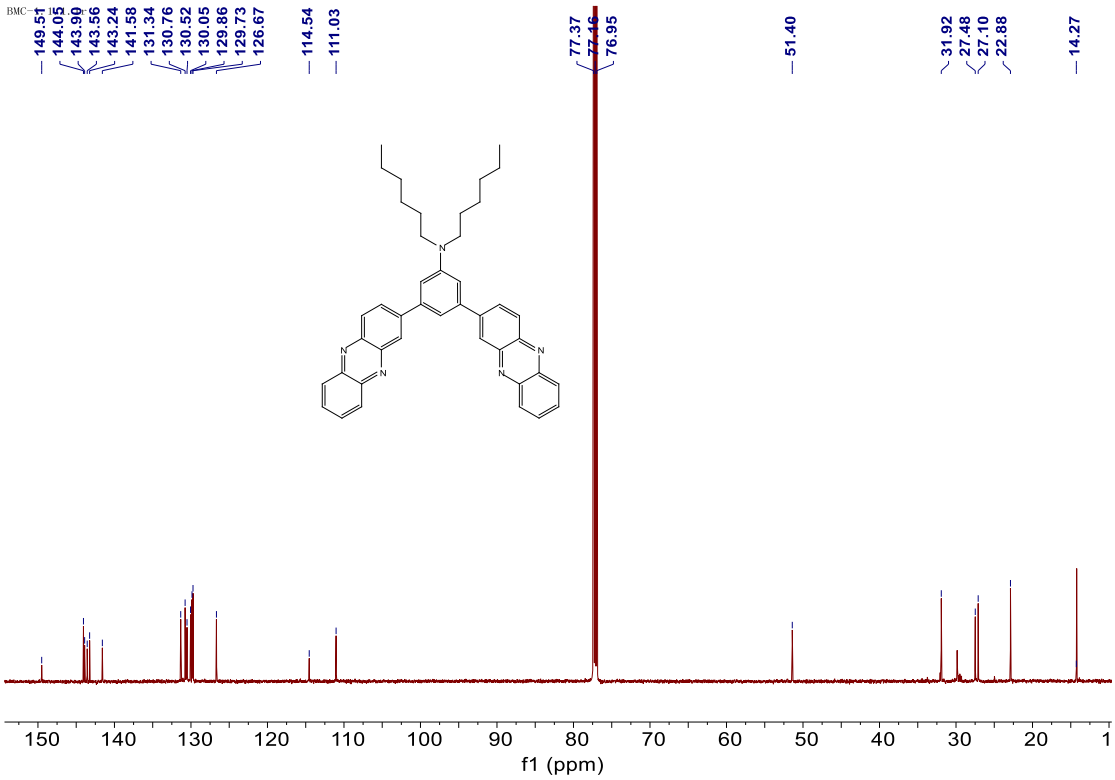

Figure S39. ^{13}C-NMR spectrum of **SMC-1** in $CDCl_3$

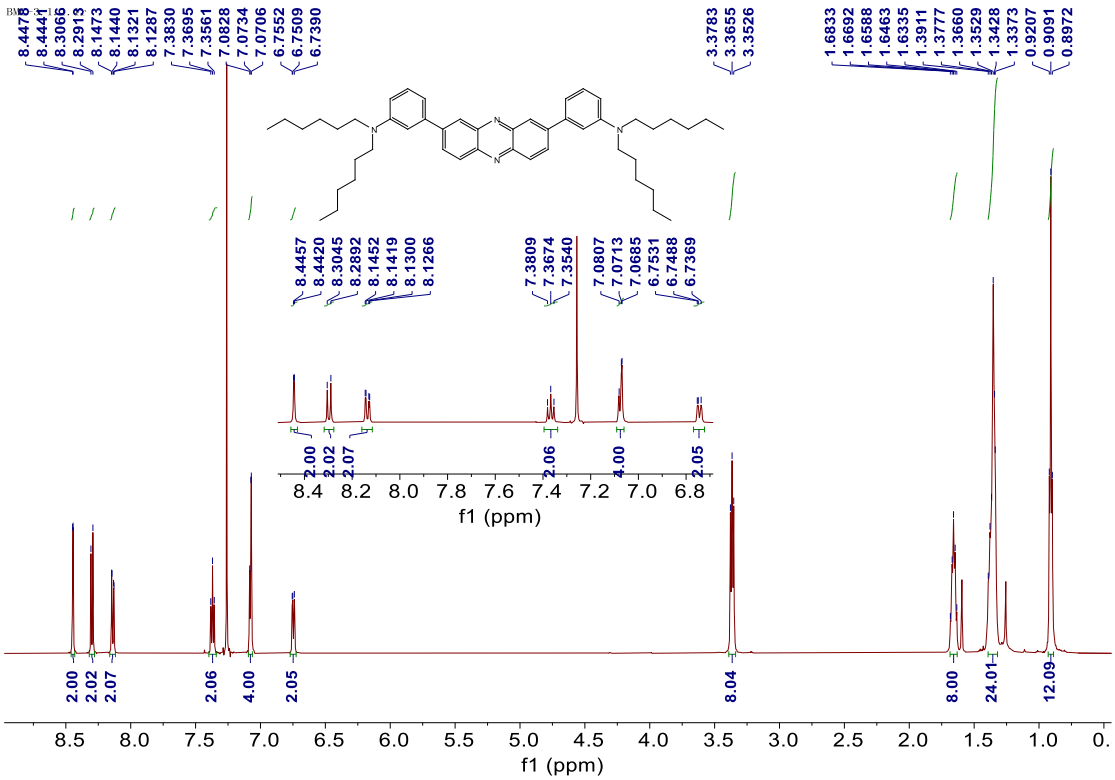

Figure S40. ^{1}H-NMR spectrum of **SMC-2** in $CDCl_3$

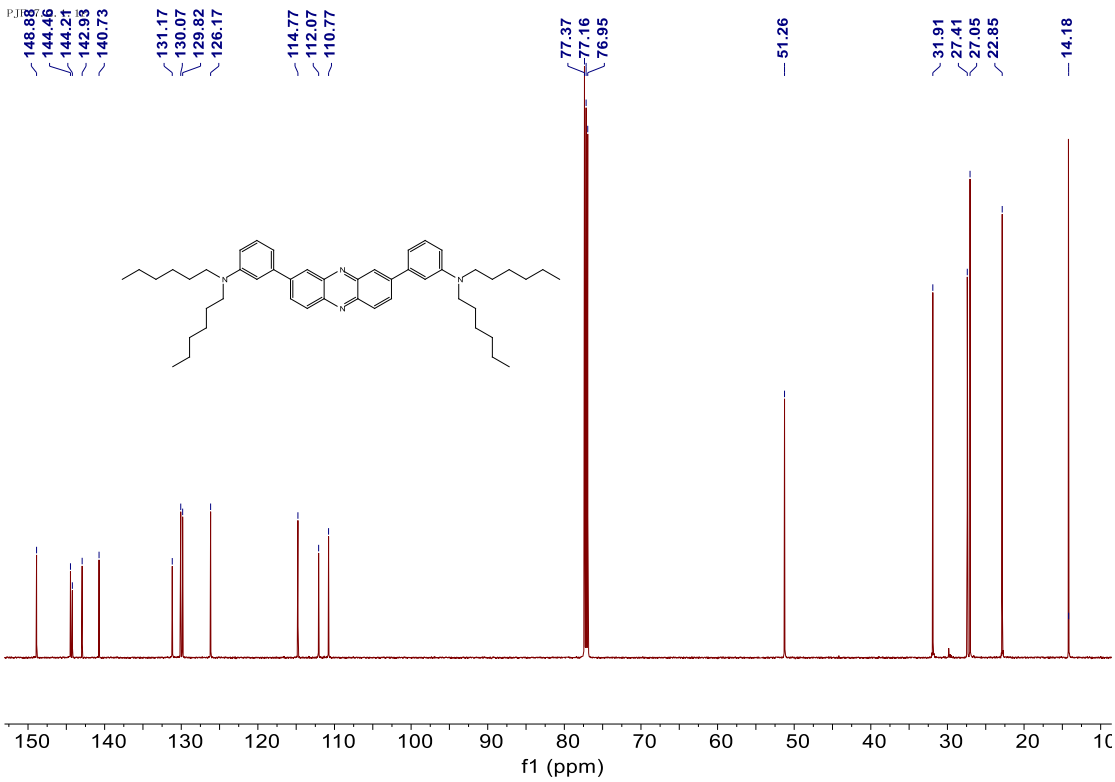

Figure S41. ^{13}C-NMR spectrum of **SMC-2** in $CDCl_3$

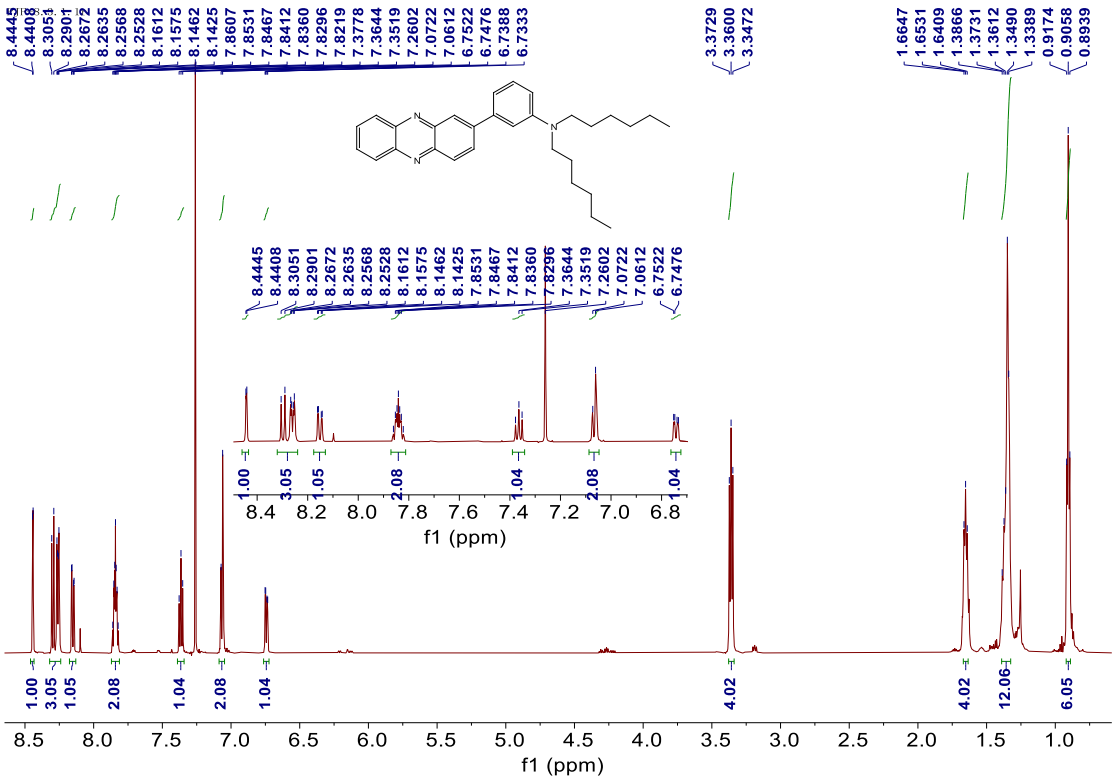

Figure S42. ^{1}H-NMR spectrum of **SMC-3** in $CDCl_3$

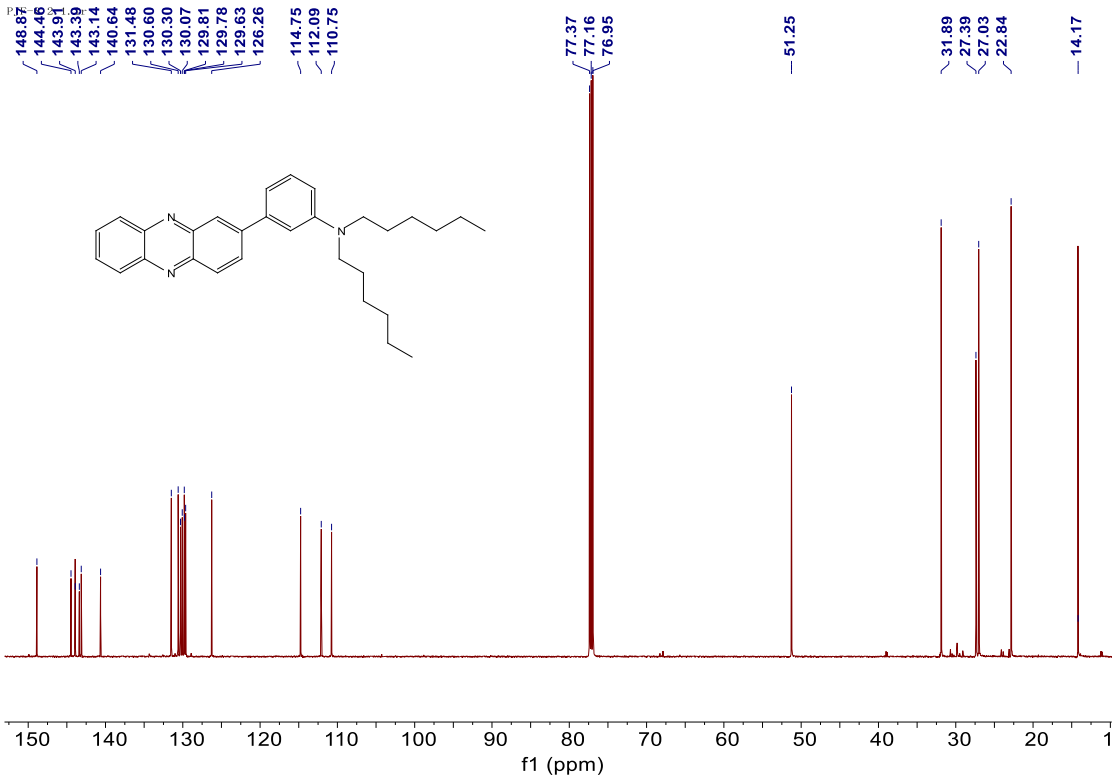

Figure S43. ^{13}C-NMR spectrum of **SMC-3** in $CDCl_3$

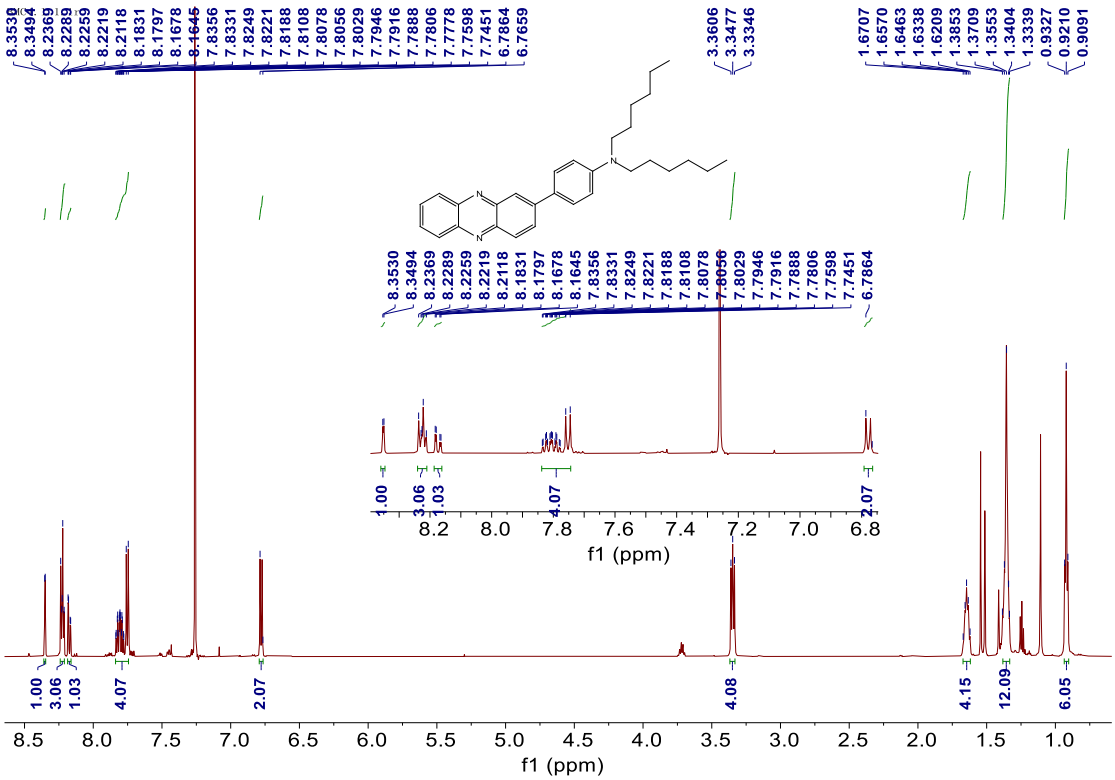

Figure S44. ^{1}H-NMR spectrum of **SMC-4** in $CDCl_3$

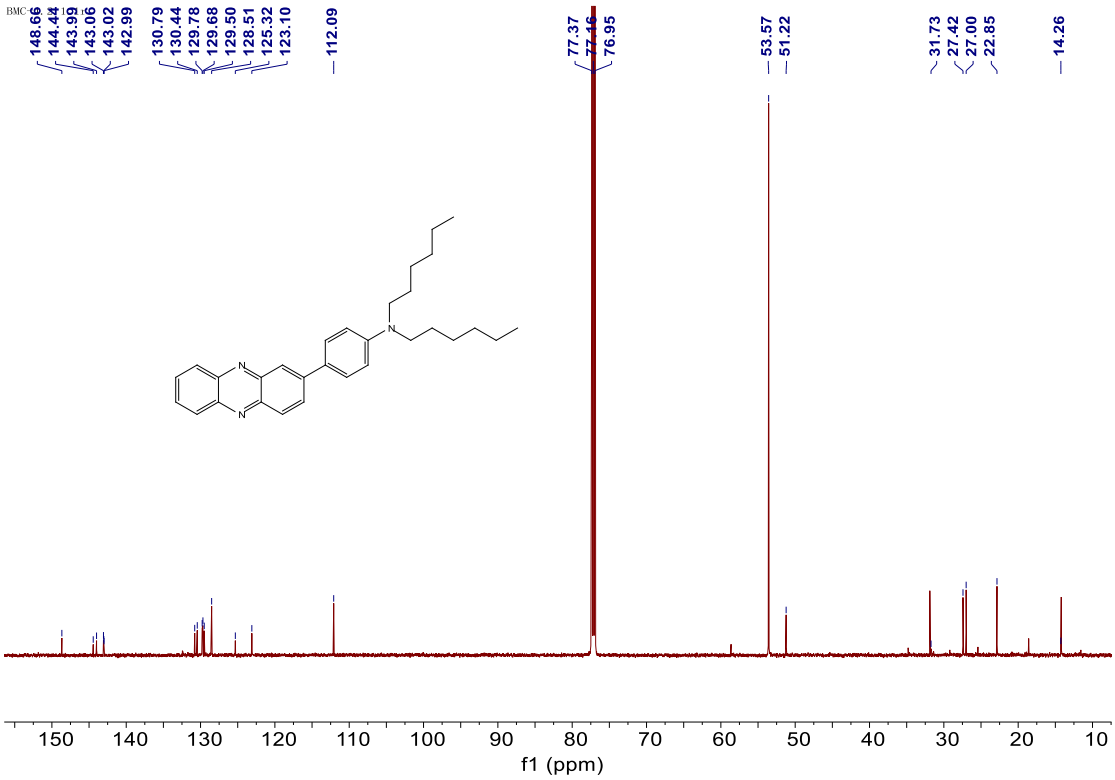

Figure S45. ^{13}C-NMR spectrum of **SMC-4** in $CDCl_3$

7. References

1. B. Y. Lu, S. Kanehashi, K. Minegishi, P. S. Wang, J. Cheng, K. Ogino, S. Li, *RSC. Adv.,* 2021, **11**, 33431-33437.
2. A. Dhara, T. Sadhukhan, G. E. Sheetz, H. A. Olsson, K. Raghavachari, H. A. Flood, *J. Am. Chem. Soc.,* 2020, **142**, 12167-12180.
3. J. M. Frisch, W. G. Trucks, B. H. Schlegel, E. G. Scuseria, A. M. Robb, R. J. Cheeseman, G. Scalmani, V. Barone, B. Mennucci, A. G. Petersson, H. Nakatsuji, M. Caricato, X. Li, P. H. Hratchian, F. A. Izmaylov, J. Bloino, G. Zheng, L. J. Sonnenberg, M. Hada, M. Ehara, K. Toyota, R. Fukuda, J. Hasegawa, M. Ishida, T. Nakajima, Y. Honda, O. Kitao, H. Nakai, T. Vreven, A. J. Montgomery, E. J. Peralta, Jr., F. Ogliaro, M. Bearpark, J. J. Heyd, E. Brothers, N. K. Kudin, N. V. Staroverov, R. Kobayashi, J. Normand, K. Raghavachari, A. Rendell, C. J. Burant, S. S. Iyengar, J. Tomasi, M. Cossi, N. Rega, M. J. Millam, M. Klene, E. J. Knox, B. J. Cross, V. Bakken, C. Adamo, J. Jaramillo, R. Gomperts, E. R. Stratmann, O. Yazyev, J. A. Austin, R. Cammi, C. Pomelli, W. J. Ochterski, L. R. Martin, K. Morokuma, G. V. Zakrzewski, A. G. Voth, P. Salvador, J. J. Dannenberg, S. Dapprich, D. A. Daniels, O. Farkas, B. J. Foresman, V. J. Ortiz, J. Cioslowski, J. D. Fox, Gaussian 09, v D.01; Gaussian, Inc.: Wallingford, CT, 2009.
4. G. Liao, C. Zheng, D. Xue, C. Fan, G. Liu, S. Pu, *RSC. Adv.,* 2016, **6**, 34748-34753.